Gastroenterology 2021;160:362–377

Targeting DNA Damage Response and Replication Stress in Pancreatic Cancer

Stephan B. Dreyer,[1,2] Rosie Upstill-Goddard,[1] Viola Paulus-Hock,[3] Clara Paris,[4] Eirini-Maria Lampraki,[1] Eloise Dray,[5] Bryan Serrels,[1,6] Giuseppina Caligiuri,[1] Selma Rebus,[1] Dennis Plenker,[7,8] Zachary Galluzzo,[7,8] Holly Brunton,[1] Richard Cunningham,[1] Mathias Tesson,[3] Craig Nourse,[3] Ulla-Maja Bailey,[1] Marc Jones,[9] Kim Moran-Jones,[10] Derek W. Wright,[1] Fraser Duthie,[1,11] Karin Oien,[1,11,12] Lisa Evers,[1] Colin J. McKay,[1,2] Grant A. McGregor,[3] Aditi Gulati,[13] Rachel Brough,[13] Ilirjana Bajrami,[13] Stephan Pettitt,[13] Michele L. Dziubinski,[14] Juliana Candido,[15] Frances Balkwill,[15] Simon T. Barry,[16] Robert Grützmann,[17] Lola Rahib,[18] Glasgow Precision Oncology Laboratory,[19], Australian Pancreatic Cancer Genome Initiative[20], Amber Johns,[21] Marina Pajic,[21] Fieke E. M. Froeling,[8,22] Phillip Beer,[23] Elizabeth A. Musgrove,[1] Gloria M. Petersen,[24] Alan Ashworth,[11,25] Margaret C. Frame,[6] Howard C. Crawford,[14] Diane M. Simeone,[26] Chris Lord,[13] Debabrata Mukhopadhyay,[27] Christian Pilarsky,[17] David A. Tuveson,[7,8] Susanna L. Cooke,[1] Nigel B. Jamieson,[1,2] Jennifer P. Morton,[1,3] Owen J. Sansom,[1,5] Peter J. Bailey,[3] Andrew V. Biankin,[1,2,28,§] and David K. Chang[1,2,28,§]

[1]Wolfson Wohl Cancer Research Centre, Institute of Cancer Sciences, University of Glasgow, Glasgow, Scotland, United Kingdom; [2]West of Scotland Pancreatic Unit, Glasgow Royal Infirmary, Glasgow, United Kingdom; [3]Cancer Research UK Beatson Institute, Glasgow, United Kingdom; [4]Department of Pharmacological Faculty, Université Grenoble Alpes, Saint-Martin-d'Heres, France; [5]Department of Biochemistry and Structural Biology, University of Texas Health San Antonio, San Antonio, Texas; [6]Medical Research Council Institute of Genetics and Molecular Medicine, Edinburgh Cancer Research UK Centre, University of Edinburgh, Edinburgh, United Kingdom; [7]Cold Spring Harbor Laboratory, Cold Spring Harbor, New York; [8]Lustgarten Foundation Pancreatic Cancer Research Laboratory, Cold Spring Harbor, New York; [9]Stratified Medicine Scotland, Queen Elizabeth University Hospital, Glasgow, United Kingdom; [10]College of Medicine, Veterinary, and Life Sciences, University of Glasgow, Glasgow, United Kingdom; [11]Department of Pathology, Queen Elizabeth University Hospital, Glasgow, United Kingdom; [12]Greater Glasgow and Clyde Bio-repository, Pathology Department, Queen Elizabeth University Hospital, Glasgow, United Kingdom; [13]Cancer Research UK Gene Function Laboratory and Breast Cancer Now Toby Robins Research Centre, The Institute of Cancer Research, London, United Kingdom; [14]Department of Molecular and Integrative Physiology, University of Michigan, Ann Arbor, Michigan; [15]Barts Cancer Institute, Queen Mary University of London, London, United Kingdom; [16]Bioscience, Oncology, Innovative Medicines and Early Development Biotech Unit, AstraZeneca, Cambridge, United Kingdom; [17]Department of Surgery, Universitätsklinikum Erlangen, Erlangen, Germany; [18]Pancreatic Cancer Action Network, Manhattan Beach, California; [19] Glasgow Precision Oncology Laboratory, Glasgow, United Kingdom; [20]Australian Pancreas Genome, Darlinghurst, Australia; [21]The Kinghorn Cancer Centre, Darlinghurst and Garvan Institute of Medical Research, Sydney, Australia; [22]Epigenetics Unit, Department of Surgery and Cancer, Imperial College London, Hammersmith Campus, London, United Kingdom; [23]Sanger Institute, Wellcome Genome Campus, Cambridge, United Kingdom,[24]Mayo Clinic, Rochester, Minnesota; [25]University of California–San Francisco Helen Diller Family Comprehensive Cancer Center, San Francisco, California; [26]Pancreatic Cancer Center, Perlmutter Cancer Center, New York University Langone Health, New York, New York; [27]Department of Biochemistry and Molecular Biology, Mayo Clinic College of Medicine and Science, Jacksonville, Florida; and [28]South Western Sydney Clinical School, Faculty of Medicine, University of New South Wales, Liverpool, Australia.

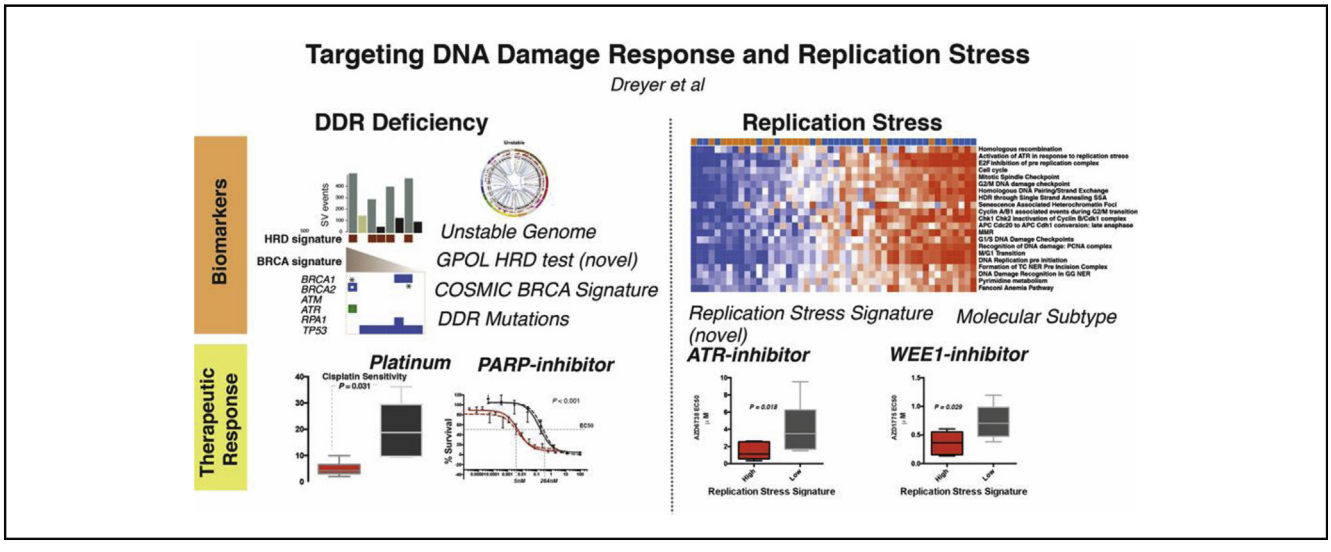

BACKGROUND & AIMS: Continuing recalcitrance to therapy cements pancreatic cancer (PC) as the most lethal malignancy, which is set to become the second leading cause of cancer death in our society. The study aim was to investigate the association between DNA damage response (DDR), replication stress, and novel therapeutic response in PC to develop a biomarker-driven therapeutic strategy targeting DDR and replication stress in PC. **METHODS:** We interrogated the transcriptome, genome, proteome, and functional characteristics of 61 novel PC patient–derived cell lines to define novel therapeutic strategies targeting DDR and replication stress. Validation was done in patient-derived xenografts and human PC organoids. **RESULTS:** Patient-derived cell lines faithfully recapitulate the epithelial component of pancreatic tumors, including previously described molecular subtypes. Biomarkers of DDR deficiency, including a novel signature of homologous recombination deficiency, cosegregates with response to platinum ($P < .001$) and PARP inhibitor therapy ($P < .001$) in vitro and in vivo. We generated a novel signature of replication stress that predicts response to ATR ($P < .018$) and WEE1 inhibitor ($P < .029$) treatment in both cell lines and human PC organoids. Replication stress was enriched in the squamous subtype of PC ($P < .001$) but was not associated with DDR deficiency. **CONCLUSIONS:** Replication stress and DDR deficiency are independent of each other, creating opportunities for therapy in DDR-proficient PC and after platinum therapy.

Keywords: Pancreatic Cancer; DNA Damage Response; Replication Stress; Personalized Medicine.

WHAT YOU NEED TO KNOW

BACKGROUND AND CONTEXT

Pancreatic cancer (PC) remains a highly lethal malignancy with few successful therapeutic options. There is a growing list of novel agents that target DNA replication and repair, which may offer treatment options for patients with PC.

NEW FINDINGS

A subset of PC demonstrate evidence of high replication stress. This is enriched in the squamous transcriptomic subtype of PC. A novel transcriptomic signature of replication stress predicts response to novel ATR and WEE1 inhibitors. High replication stress and DNA damage response (DDR) deficiency are separate entities that can exist independently and be targeted with different agents.

LIMITATIONS

This study is limited that the novel therapeutic data is based on preclinical models of patient derived cell lines and organoid responses. Human PC response data is not yet available, as the ATR and WEE1 inhibitors are at early stages of therapeutic development in PC.

IMPACT

High replication stress and DDR deficiency exist independently of each other, offering therapeutic opportunities in DDR proficient PC with high replication stress using ATR or WEE1 inhibitors. It also provides a potential therapeutic strategy in the acquired platinum resistance setting.

Pancreatic cancer (PC) has recently overtaken breast cancer to become the third leading cause of cancer death in the United States,[1] and it is predicted to become the second within a decade.[2] Pancreatic ductal adenocarcinoma (PDAC), the more common form of PC, is dominated by mutations in 4 well-known cancer genes (*KRAS*, *TP53*, *CDKN2A*, and *SMAD4*). Only a few genes are mutated in 5%–15% of cases, amidst an ocean of infrequently mutated genes in the majority of patients.[3–11] This diversity may explain the lack of progress with targeted therapies, because actionable genomic events being targeted therapeutically are present in only a small proportion of unselected participants in clinical trials.[12] To better select patients to clinical trials, biomarkers that predict response to novel and established treatments are urgently needed and must extend beyond the detection of point mutations in coding genes and low-prevalence actionable genomic events.

Although molecular subtyping of cancer based on biological attributes can facilitate drug discovery, to be clinically relevant, the optimal taxonomy must inform patient management through prognostication or, more importantly, treatment selection.[13] Recent studies have subtyped PC in various ways,[5,9,14–18] grouping similarities based on structural attributes of genomes, genes mutated in pathways, or molecular mechanisms inferred through messenger RNA expression. We recently defined 4 transcriptomic subtypes of PC,[5,19] with 2 distinct primary lineages, termed *classical pancreatic* (which can be further divided into pancreatic progenitor, immunogenic, and aberrantly differentiated endocrine exocrine subtypes) and *squamous*.[5] Despite discrepancies in nomenclature, 1 molecular class (variably termed *quasi-mesenchymal*, *basal-like*, or *squamous*) is consistently defined and is associated with a poor prognosis.[19,20] A key distinction is the epigenetic profile of the squamous subtype, with chromatin modification and methylation orchestrating the loss of pancreatic endodermal transcriptional networks and, as a consequence, suppressing transcripts that designate a pancreatic identity.[5] These biologically based molecular taxonomies of PC, although associated with differences in outcome, have yet to inform treatment decisions.

§ Authors share co-senior authorship.

Abbreviations used in this paper: **DDR, DNA damage response; DMSO, dimethyl sulfoxide; EC_{50}, median effective concentration; GO, Gene Ontology; HR, homologous recombination; HRD, homologous recombination deficiency; ICGC, International Cancer Genome Consortium; MTS, 3-(4,5-dimethylthiazol-2-yl)-5-(3-carboxymethoxyphenyl)-2-(4-sulfophenyl)-2H-tetrazolium; PC, pancreatic cancer; PDAC, pancreatic ductal adenocarcinoma; PDCL, patient-derived cell line; PDX, patient-derived xenograft; RNAseq, RNA sequencing; RPPA, reverse-phase protein array; siRNA, small interfering RNA; SV, structural variation; TOM, topological overlap measure.**

Most current article

© 2021 by the AGA Institute. Published by Elsevier Inc. This is an open access article under the CC BY license (http://creativecommons.org/licenses/by/4.0/).

0016-5085
https://doi.org/10.1053/j.gastro.2020.09.043

DNA damage response (DDR) deficiency is a hallmark of cancer, including PC,[8] and is thought to render some tumors preferentially sensitive to DNA-damaging agents such as platinum and PARP inhibitors. There is a growing compendium of novel therapeutics that target DNA damage response mechanisms and the cell cycle, such as ATR and WEE1 inhibitors.[21] Genomic instability, a key feature of many cancers, typically secondary to defects in DNA replication and repair during the cell cycle, often results in replication stress.[22,23] Oncogene activation drives replication stress, particularly through RAS and MYC signaling, both of which are prevalent molecular features of PC.[22,24,25] The platinum-containing regimen, FOLFIRINOX, has become the standard of care for all stages of PC, yet it is suitable only for patients with good performance status; however, the majority of patients unfortunately do not respond.[26–28] Consequently, many patients experience the morbidity, and even mortality, of systemic platinum chemotherapy with little or no survival benefit or quality of life. Biomarker-driven patient selection strategies and novel therapeutics that build on platinum response or disease stabilization that target DDR mechanisms provide a substantial opportunity to improve outcomes.

Building on previous work on DDR mechanisms and PC, we aim to expand the indications for novel DDR inhibitors beyond patients with defects in homologous recombination (HR) mechanisms. We aim to refine proposed DDR biomarkers of platinum response to be tested in prospective clinical trials and to correlate and overlap this with cell cycle inhibitor response to identify patients who will respond to novel agents, such as ATR and WEE1 inhibitors.

Here, we used 61 patient-derived cell lines (PDCLs) of PC (Supplementary Tables 1 and 2) to define subtype-specific molecular mechanisms and identify opportunities for molecular subtype–directed treatment selection that targets DDR mechanisms. We performed messenger RNA expression analysis (RNA sequencing [RNAseq]) (n = 48) complemented by whole genome sequencing (n = 47), which was further enhanced with reverse phase protein arrays (RPPAs), functional screenings using small interfering RNA (siRNA) and targeted functional analysis. To our knowledge, we identify novel biomarkers of DDR deficiency and replication stress with potential clinical utility that associate with therapeutic sensitivity. We show that DDR deficiency exists independently of replication stress, the previously identified poor-prognostic squamous subtype is enriched for replication stress, and transcriptomic readouts of replication stress confer sensitivity to therapeutics that target the cell cycle checkpoint machinery.

Materials and Methods

The full methods and additional references can be found in the Supplementary Material.

Human Research Ethics Approvals

Ethical approval was obtained for all human samples and data (Supplementary Materials).

Cell Culture

PDCLs were generated as previously described.[4,29–31] PDCLs were cultured in conditions specifically formulated for each individual line based on growth preferences and those resulting in cell lines that most closely resembled physiologic cells from the initial tumor. Cells were grown in a humidified environment with either 5% or 2% CO_2 at 37°C. All cell lines were profiled by short tandem repeat DNA profiling as unique (CellBankaustralia.com). Cell lines were tested routinely for mycoplasma contamination by using the MycoAlert PLUS Mycoplasma Detection Kit (Lonza, Basel, Switzerland; LT07–318).

In Vitro Cytotoxicity Assays

Cells were seeded on 96-well plates (Costar, Corning, Corning, New York) and allowed to adhere for 24 hours. Cells were treated with increasing doses of cisplatin (Accord Healthcare, London, UK), AZD6738 (AstraZeneca, Cambridge, UK), AZD1775 (AstraZeneca), and AZD7762 (AstraZeneca) for 72 hours. Cells were treated with BMN-673 (Pfizer, New York, NY), Rucaparib (Clovis Oncology, Boulder, CO), CFI-400945 (Cayman Chemical, Ann Arbor, MI), and Palbociclib (Pfizer) for a total of 9 days, with repeated dosing every 72 hours in conjunction with changing cell media. Actinomycin D (Sigma-Aldrich, St Louis, MO), drug vehicle (dimethyl sulfoxide [DMSO]), and media-only controls were performed on each individual plate. For all other cytotoxicity assays, cells were plated in 96-well plates and treated with serial dilutions of indicated inhibitors 24 hours after plating for the indicated timepoints. Cell viability was determined by using the CellTiter 96 Aqueous nonradioactive cell proliferation assay (PROMEGA, United Kingdom) composed of solutions of a tetrazolium compound (3-[4,5-dimethylthiazol-2-yl]-5-[3-carboxymethoxyphenyl]-2-[4-sulfophenyl]-2H-tetrazolium, inner salt; [MTS]) and an electron-coupling reagent (phenazine methosulfate) (Promega, Madison, WI). The assay was performed at an absorbance of 490 nm using an enzyme-linked immunosorbent assay plate reader (Tecan Trading AG, Männedorf, Germany). Background absorbance was corrected for by wells containing medium alone, and the absorbance was normalized to a scale of 0% (complete cell death by actinomycin D (5–10 μg/mL) to 100% (no drug). At least 3 biological repeats were performed for each experiment. Median effective concentration calculation and dose response curves were generated with GraphPad Prism 6 (GraphPad Software, La Jolla, CA).

Organoid Drug Screening

Therapeutic sensitivity in the organoids was assessed as previously described.[32] Organoids were dissociated into single cells. One thousand viable cells were plated per well in 20 μL 10% Matrigel/human complete organoid media (Corning Life Sciences, United Kingdom). Increasing concentrations of AZD6738 (AstraZeneca) and AZD1775 (AstraZeneca) were added 24 hours after plating, after the reformation of organoids was visually verified. Compounds were dissolved in DMSO, and all treatment wells were normalized to 0.5% DMSO content. After 7 days, cell viability was assessed by using CellTiter-Glo (Promega) as per the manufacturer's instructions on a SpectraMax I3 (Molecular Devices, San Jose, CA) plate reader. At

least 3 biological repeats were performed for each experiment. Median inhibitory concentration calculation and dose response curves were generated with GraphPad Prism 6.

Patient-Derived Xenografts

Patient-derived xenografts (PDXs) of PDAC were generated and comprehensively characterized as part of the International Cancer Genome Consortium (ICGC) project. BALB/c nude mice were anesthetized, and a single PDX fragment was inserted subcutaneously into the right flank according to standard operating procedure. PDX models were grown to 150 mm^3 (volume = [length^2 × width]/2); at this point, each PDX was randomized to a different treatment regimen. Responsive PDXs were treated once tumor size returned to 150 mm^3, up to a maximum of 3 rounds. Resistant models were treated after a treatment break of 2 weeks in accordance with current clinical treatment regimes, up to a maximum of 2 rounds. Each experiment was terminated once tumor volume reached the endpoint (750 mm^3), in accordance with home office animal welfare regulations. Full methods can be found in Supplementary Materials.

γH2AX and pRPA Foci Formation Assay

PDCLs were cultured as standard and seeded in 96-well plates at a concentration of 10^4 cells per well. At 24 hours after seeding, cells were either left untreated or exposed to 4 Gy of ionizing radiation and processed for analysis at 2, 4, and 20 hours after exposure. Cells were stained with primary antibodies at a dilution of 1:1000 with anti-pRPA32 (S4/S8; Bethyl Laboratories, Montgomery, TX) and anti-γH2AX (Ser139; Merck, Kenilworth, NJ). Secondary antibodies used were Alexa 488 anti-mouse IgG (green) and Cy3 anti-rabbit IgG (Sigma-Aldrich). 4′,6-Diamidino-2-phenylindole (Life Technologies, Rockville, MD) was used as a nuclear stain. Confocal imaging was performed by using the Opera Phenix high-content screening system (PerkinElmer, Waltham, MA) at ×63 magnification using a water objective, at wavelengths of 405 nm (4′,6-diamidino-2-phenylindole), 488 nm (Alexa), and 561 nm (Cy3). A minimum of 320 cells (median, 980; range, 322–1886), in 2 separate experiments, were analyzed for each time point. Image analysis was performed by using the Columbus Image data storage and analysis system (PerkinElmer). Statistical analysis was performed with GraphPad Prism 6.

Nucleic Acid Extraction

DNA and RNA extraction were performed by using previously published methods.[4]

Whole-Genome Library Preparation

Whole-genome libraries were generated by using either the Illumina (San Diego, CA) TruSeq DNA LT sample preparation kit (part nos. FC-121–2001 and FC-121–2001) or the Illumina TruSeq DNA PCR-Free LT sample preparation kit (Illumina, part nos. FC-121–3001 and FC-121–3002) according to the manufacturer's protocols with some modifications (Illumina, part no. 15026486 Rev. C July 2012 and 15036187 Rev. A January 2013 for the 2 different kits, respectively). Full methods can be found in the Supplementary Materials.

RNA Sequencing Library Generation and Sequencing

RNA-seq libraries were generated by using the Illumina TruSeq Stranded Total RNA (part no. 15031048 Rev. D April 2013) kits on a Perkin Elmer Sciclone G3 NGS Workstation (product no. SG3-31020-0300). Full methods can be found in the Supplementary Material.

Library Sequencing

All libraries were sequenced by using the Illumina HiSeq 2000/2500 system with TruSeq SBS Kit v3-HS (200 cycles) reagents (part no. FC-401-3001) to generate paired-end 101–base pair reads.

Copy Number Analysis

Matched tumor and normal patient DNA was assayed by using Illumina SNP BeadChips as per manufacturer's instructions (HumanOmni1-Quad or HumanOmni2.5–8 BeadChips) and analyzed as previously described.

Identification and Verification of Structural Variants

The somatic structural variant pipeline was identified by using the qSV tool. A detailed description of its use has been recently published.[4,33]

Identification of and Verification of Point Mutations

Substitutions and insertions/deletions were called by using a consensus calling approach that included qSNP, GATK, and Pindel. The details of call integration and filtering and verification using orthogonal sequencing and matched sample approaches are as previously described.[4,33,34]

Mutational Signatures

Mutational signatures were defined for genome-wide somatic substitutions, as previously described.[4]

HRDetect

HRDetect scores were calculated as previously described for the PDCLs.[35]

Small Interfering RNA Screening and Analysis

Full siRNA screening and analysis were performed with established methods and are described in the Supplementary Material.

Reverse-Phase Protein Array

RPPA was performed to investigate proteomic differences between PDCLs by using established methods and is fully described in the Supplementary Materials.

RNA-Sequencing Analysis

RNA-seq read mapping was performed by using the bcbio-nextgen project RNAseq pipeline (https://bcbio-nextgen.readthedocs.org/en/latest/). Briefly, after quality control and

adaptor trimming, reads were aligned to the GRCh37 genome build by using STAR counts for known genes, which were generated with the function featureCounts in the R (R Foundation for Statistical Computing, Vienna, Austria)/Bioconductor package Rsubread. The R/Bioconductor package DESeq2 was used to normalize count data among samples and to identify differentially expressed genes. Expression data were normalized by using the rlog transform in the DESeq2 package, and these values were used for all downstream analyses.

Weighted Gene Coexpression Network Analysis

Weighted gene coexpression network analysis was used to generate a transcriptional network from rlog-normalized RNAseq data. Briefly, weighted gene coexpression network analysis clusters genes into network modules by using a topological overlap measure (TOM). The TOM is a highly robust measure of network interconnectedness and essentially provides a measure of the connection strength between 2 adjacent genes and all other genes in a network. Genes are clustered by using 1 – TOM as the distance measure, and gene modules are defined as branches of the resulting cluster tree using a dynamic branch-cutting algorithm. Full methods can be found in the Supplementary Materials.

Identification of Significant Subtype-Specific Changes in Pathways and/or Processes

The R package clipper was used to identify pathways and/or processes showing significant change between PDCL subtypes. clipper implements a 2-step empirical approach, using a statistical analysis of means and concentration matrices of graphs derived from pathway topologies, to identify signal paths having the greatest association with a specific phenotype.

Pathway Analysis

Ontology and pathway enrichment analysis was performed by using the R package dnet and/or the ClueGO/CluePedia Cytoscape plugins, as indicated. Visualization and/or generation of network diagrams was performed using either Cytoscape or the R package RedeR.

Glasgow Precision Oncology Laboratory Homologous Recombination Deficiency Test

Signature generation was done by using whole-genome sequencing data as previously described.[36,37] A positive test was defined when the following criteria were met.

1. There were more than 50 structural variants in total.
2. Greater than 70% of the structural variants were deletions, duplications, or translocations.
3. The structural variation (SV) pattern was not focal, as defined by a large number of structural variants due to chromothripsis or amplifications.
4. If the predominant variant types were deletions and translocations, the median deletion size was <10 kilo base pairs.

OR

5. If the predominant variant type was duplication, the median duplication size was <50 kilo base pairs.

Replication Stress Signature Generation

Differentially expressed genes were compared to genes associated with Gene Ontology (GO) terms using the R package dnet. Significantly expressed GO terms involved in DNA damage response and cell cycle control were selected. Differential expression of each selected GO term was applied to each individual PDCL and patient derived organoid that underwent RNAseq. This, in turn, was used to generate a composite score by totaling the score for each selected GO term sig.score. The function from the R package genefu was used to calculate a specific signature score in a given sample using the signatures generated for each pathway and/or process. This was termed the *replication stress signature*. Generation of the signature score for bulk tumor samples followed the same methodology.

Bulk Expression Sets and Immune Signature Scores

Bulk RNAseq expression data, subtype assignments, and immune signature scores were obtained from Bailey et al.[5]

Gene Set Enrichment of Pancreatic Ductal Adenocarcinoma Subtypes

Gene set enrichment was performed by using the R package GSVA. Gene sets representing PDAC subtypes were generated as previously described.

Clustering and Subtype Assignment

The package ConsensusClusterPlus was used to classify PDCLs according to the expression signatures defined by Moffitt et al[18] and Bailey et al.[5] Gene sets representing PDAC subtypes were generated as previously described.

Statistical Analysis

A Kruskal-Wallis test was applied to the indicated stratified scores to determine whether distributions were significantly different. Fisher exact tests were used to evaluate the association between dichotomous variables.

Plot Generation

Heatmaps and oncoplots were generated by using the R package ComplexHeatmap. Dot charts, density plots, and boxplots were generated using the R package ggpubr. Violin plots were generated with the Python package Seaborn. Biplot was generated with the R package ggfortify. All other plots were generated with the R package ggplot2.

Results

Patient-Derived Cell Lines Recapitulate Pancreatic Cancer Subtypes

Hierarchical clustering of RNAseq data from the 48 PDCLs recapitulated the 2 primary classes of PC (Figure 1*A*, Supplementary Figure 1, and Supplementary Tables 3-5). Twenty-eight (58%) of the PDCLs were classified as squamous, and 20 (42%) were classical (Supplementary Table 4). The preservation of the 26 transcriptional networks (Gene Programs) we previously

described in bulk PC[5] was compared to PDCL-derived gene programs (Supplementary Figure 1 and Supplementary Tables 6 and 7). In total, 17 of the 26 gene programs were closely recapitulated in the PDCLs (Supplementary Figure 1), with the expected absence of immune infiltrate–related transcriptional networks (Supplementary Table 7). The lack of stroma permitted higher resolution of epithelial transcriptomic networks, showing key mechanisms that are difficult to discern from biopsy samples. Differential expression of genes related to DNA damage response, cell cycle control, and morphogenic processes were observed between subtypes and correlated in both PDCLs and bulk tumor samples (Figure 1*A*). These findings suggest that PDCLs are representative of bulk PC and can be used to develop novel DDR therapeutic strategies for the clinic and that epithelial cell purity can provide greater sensitivity in detecting aberrant mechanisms.

Biomarkers of DNA Damage Response Deficiency in Pancreatic Ductal Adenocarcinoma of Pancreatic Cancer

Various biomarkers of DDR deficiency associated with therapeutic response have been proposed but not validated clinically in PC. High-ranking Catalogue of Somatic Mutations in Cancer (COSMIC) Breast Cancer gene (BRCA) point mutational signature cosegregates with a high prevalence of structural variants, termed the *unstable* genomic subtype, and deleterious mutations in HR repair pathway genes such as *BRCA1* and *2* and *PALB2*[4] (Figure 1*B* and Supplementary Tables 8-10). We previously showed that these signatures are associated with retrospective clinical response to platinum in PC.[4] More recently, early data also suggest a therapeutic signal using PARP inhibitors; however, efficacy is not well defined beyond *BRCA1/2* mutations.[36,37] To address this, we defined PDCLs as DDR deficient based on the presence of any of 4 putative biomarkers: (1) SV number and pattern (>200 SVs = unstable genome), (2) a high COSMIC BRCA mutational signature (ranked within top quintile), (3) a positive GPOL HR deficiency (HRD) test,[38,39] and (4) mutations in key DDR genes (*BRCA1*, *BRCA2*, *ATM*, *ATR*, *RPA1*, *RAD51*, *RAD54*, and *FANCA*) (Figure 1*B*, Supplementary Figure 2, and Supplementary Table 11). Out of 47 PDCLs with whole-genome sequencing data, 6 (13%) had a positive GPOL HRD test result; 9 (19%) had >200 SVs (unstable genome); and 10 (21%) had mutations in DDR genes, of which 2 were germline variants (both in *BRCA2*) (Figure 1*B*, and Supplementary Table 12). There were 4 PDCLs with homozygous mutations in either *BRCA1*, *BRCA2*, or *RPA1*; these were all associated with unstable genomes, and 3 of these were positive on GPOL HRD test (Figure 1*B* and)Supplementary Table 3. Significant overlap existed among these, with n = 3 PDCLs with all 4 biomarkers present; n = 1 had 3 (unstable genome, GPOL HRD test, BRCA mutational signature) biomarkers positive, n = 4 were positive for 2 biomarkers, and the remaining n = 8 had 1 biomarker positive (Supplementary Table 13). There was no association between transcriptomic subtype and DDR status ($P = .706$).

DNA Damage Response Deficiency Cosegregates With Response to Platinum and PARP Inhibitor Treatment

To investigate the relationship between these putative biomarkers of DDR deficiency and platinum and PARP inhibitor response, cell viability assays were performed on 15 PDCLs. PDCLs defined as DDR deficient were more sensitive to both cisplatin therapy ($P = .031$) and PARP inhibition ($P < .001$) compared to DDR-proficient PDCLs (Figure 2 and Supplementary Table 11). The DDR-deficient PDCLs all had median effective concentrations (EC_{50}s) to platinum of below the sensitivity threshold (10 μmol/L) set by large-scale pancancer cell line drug screenings (n = 880) using cisplatin (cancerrxgene.org [COSMIC]).

To further define clinically applicable therapeutic response biomarkers of DDR deficiency in vivo, bulk tumor PDX models that represent both DDR-proficient (PDX 2133) and -deficient (PDX 2179) PC were generated in balb/c nude mice. The DDR-proficient PDX did not respond to DNA-damaging agents, including cisplatin and the PARP inhibitor olaparib combination (Figure 2). The DDR-deficient PDX model, with a biallelic somatic loss-of-function *BRCA1* mutation, responded exceptionally to cisplatin and olaparib as monotherapy and in combination (Figure 2), suggesting that PARP inhibition can be as effective as platinum chemotherapy in DDR-deficient PC.

These results suggest that DDR deficiency, as defined by these putative biomarkers, have potential clinical utility in predicting response to platinum treatment. Importantly, this included both somatic and germline mutations, suggesting that therapeutic sensitivity extends beyond germline *BRCA1* and *2* mutations (Figure 2 and Supplementary Table 12). The most robust predictors appear to be biallelic loss-of-function mutations in *BRCA1* or *BRCA2*, or the presence of a genomic scar indicating loss of HR, such as high SVs (>200) and a positive GPOL HRD test. The COSMIC BRCA mutational signature appears to be a poor predictor of platinum response (Supplementary Figure 3).

Replication Stress Is a Feature of the Squamous Subtype of Pancreatic Cancer

Replication stress has been described to be closely related to DDR deficiency, and activation of cell cycle genes is enriched in the squamous subtype. As a consequence, we investigated targeting of replication stress as a novel therapeutic strategy. We found significant subtype differences in the expression of genes controlling cell cycle, including the G2/M checkpoint in both PDCLs and bulk tumor PC (Figure 1). Expression of *WEE1* ($P = .006$), *CDK6* ($P = .02$), and *CDK7* ($P < .001$) was enriched in the squamous subtype in both PDCLs and bulk tumor (Figure 1*A*). We then used a combination of DNA maintenance, replication, and cell cycle regulation network–related transcriptional profiles from GO and pathway enrichment analysis to define replication stress using mechanisms associated with DNA replication (ATR activation, chromosomal maintenance, E2F transcriptional pathways, HR, Fanconi anemia, base-excision repair, p53 signaling, endoplasmic reticulum stress, and RNA

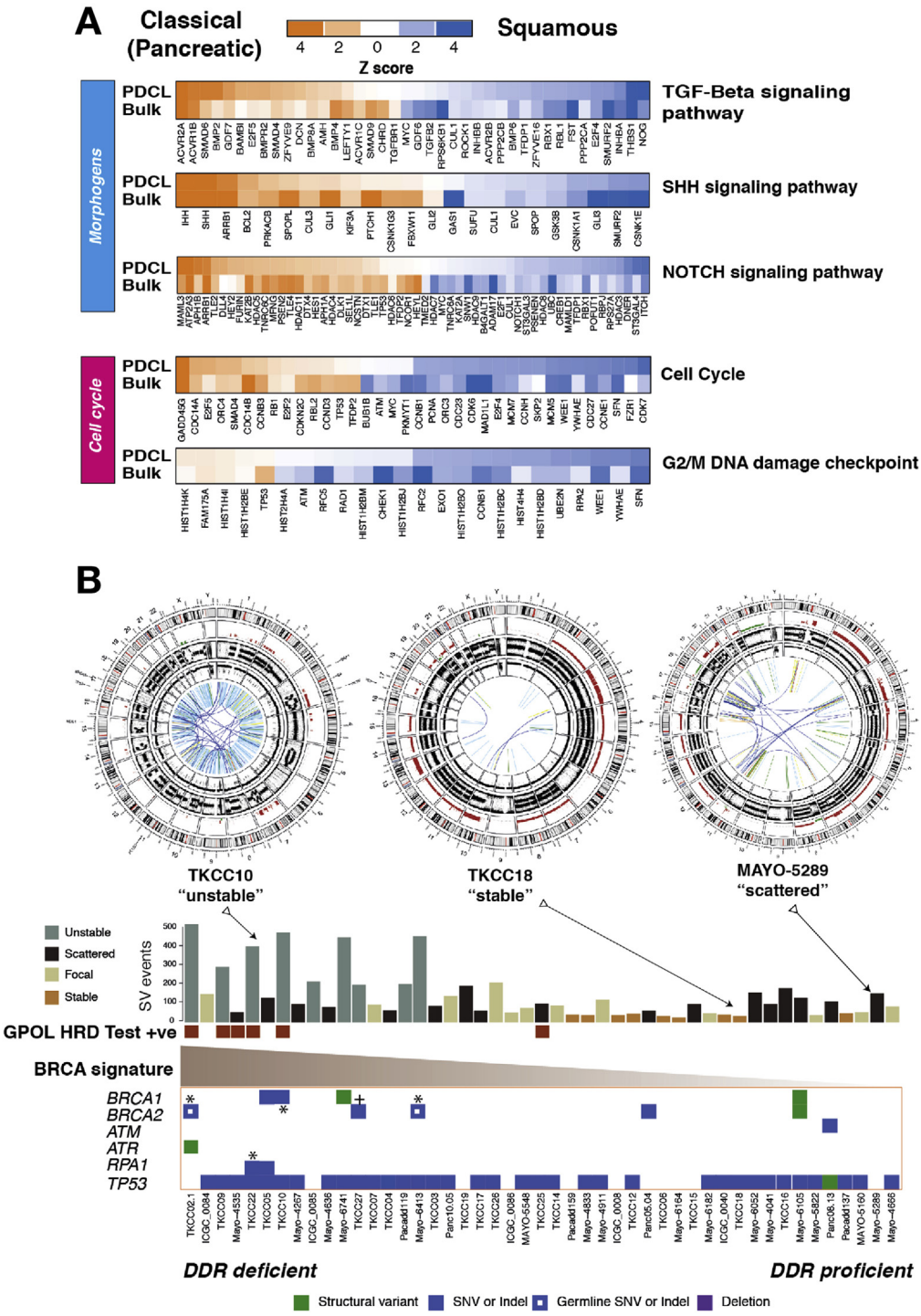

Figure 1. Subtype specific differences and DDR in PDCLs of PC. (*A*) Heatmaps of key genes in pathways important in carcinogenesis, grouped into distinct molecular processes related to morphogenesis and cell cycle control between molecular subtypes of bulk tumor and PDCLs of PC. The degree of color saturation is proportional to the degree of enrichment in the squamous (*blue*) and classical pancreatic (*orange*) subtypes. For all samples within each subtype, genes are ranked by the most differentially expressed between subtypes. (*B*) Surrogate biomarkers of DDR deficiency, defined by large-scale sequencing projects of PC, include (1) unstable genome (>200 SVs), (2) the novel GPOL HRD test, (3) high-ranking BRCA mutational signature, and (4) deleterious mutations in DDR pathway genes. PDCLs are ranked from left to right based on the COSMIC BRCA mutational signature, with SV subtype, number of SVs, and GPOL HRD test status symbolized on the top bar. Examples of circos plots for 3 PDCLs are included, representing unstable, stable, and scattered subtypes. SNV, single-nucleotide variant; TGF, transforming growth factor.

processing). This resolved into a transcriptomic signature (termed the *replication stress signature*), which was applied as a hypothetical biomarker of replication stress (Figure 3 and Supplementary Table 14).

PDCLs with high replication stress were more likely to be of the squamous subtype ($P < .001$) (Figure 3) and had significantly higher levels of pRPA at rest (a surrogate marker of single-stranded DNA break accumulation that infers replication stress) ($P < .0001$) (Figure 3). PDCLs with high replication stress and concurrent HRD had a greater proportion of γH2AX-positive cells at rest (Supplementary tables 15 and 16) (a marker of double-stranded DNA breaks) ($P = .0086$) and had persistently high levels of pRPA- and γH2AX-positive cells at 20 hours after ionizing radiation, when pRPA and γH2AX should have returned to normal levels in cells with no replication defects and competent at repairing this level of DNA damage (Supplementary Figure 4). RPPAs inferred functional consequences with differential

phosphorylation and activation of key effectors of DDR and cell cycle progression between the classical and squamous subtypes (CHK1, CHK2, Rb, $p21^{CIP1}/^{WAF1}$, ATM/ATR substrates, cyclin D1, histone H2AX) (Figure 3, Supplementary Figure 4, and Supplementary Table 15). The squamous subtype is also enriched for the activation and transcription of oncogenes including *MYC* and *CCNE* (Figure 3). Oncogene activation is known to cause replication stress secondary to genomic instability, leading to activation of cell cycle checkpoint regulatory proteins involved in the replication stress response, such as ATR, WEE1, and CHK1[25,40] (Supplementary Figure 3).

An siRNA screening targeting genes controlling DNA damage repair and replication showed a functional dependency on DDR proteins, including ATM, ATR, and CHK1 in squamous PDCLs (Figure 3*F*, Supplementary Figure 2, and Supplementary Table 17). This is in keeping with the results from the immunofluorescent and RPPA analyses suggesting higher baseline levels of proteins associated with replication stress in the squamous PDCLs and a subsequent dependency on these proteins and cell cycle checkpoints for maintaining genomic integrity and cell survival.

Differential expression of genes regulating the G2/M checkpoint in PDCLs and bulk tumors (such as *WEE1* and *CHEK1*) and the dependence on ATR activation in response to replication stress (Figure 3*A*) suggest that selective inhibition of these mechanisms may confer efficacy in tumors with high replication stress.

Replication Stress Is Associated With Sensitivity to Cell Cycle Checkpoint Inhibitors

Novel agents currently in early-phase clinical trial targeting the cell cycle were used to generate a therapeutic testing strategy (Supplementary Figure 3*B*).[41–45] Based on these data, in vitro sensitivity was assessed by using cell viability assays after a selection of PDCLs were treated with increasing doses of inhibitors of CHK1 (AZD7762), CDK4/6 (palbociclib), and PLK4 (CFI-400945), showing differential sensitivity (Supplementary Figure 3 and Supplementary Table 18). Based on promising early clinical trial results in other cancer types,[44–49] more extensive testing using inhibitors of ATR (AZD6738) and WEE1 (AZD1775) was performed on 15 PDCLs defined as high and low replication stress based on the replication stress signature score (Figure 3*A* and Supplementary Figure 3). This showed that PDCLs with high replication stress were more sensitive to both ATR and WEE1 inhibition (Figure 4*A–D*). To validate these findings, we used a panel of human PC-derived organoids,[32] which are deemed as the current criterion standard 3-dimensional model for pharmacotyping (Supplementary Tables 19 and 20). As seen in the PDCLs, organoids within the top quintile of high replication stress predicted response to both ATR and WEE1 inhibition with sensitivity to both agents in all organoids classified as high replication stress (Figure 4*E–H*). Importantly, these responses were independent of DDR status or molecular subtype, with responses seen in only high replication stress PDCLs (Supplementary Figure 3), suggesting that high replication stress signature is a more reliable biomarker of ATR inhibitor or WEE1 inhibitor response than squamous subtype or DDR deficiency.

Replication Stress Is Independent of DNA Damage Response Deficiency in Pancreatic Cancer

To investigate the relationship of replication stress and DDR deficiency and the alignment of these therapeutic segments, a comparison was performed with the PDCL cohort. By using the described biomarkers of DDR deficiency and replication stress, a 2-by-2 grid was constructed to compare replication stress ranking and DDR deficiency (Figure 5). This showed that signatures of DDR deficiency and replication stress are largely independent of each other, yet high replication stress is enriched in the squamous subtype ($P = .007$) (Figure 5). Therapeutic response data were overlapped based on previously described experiments by using ATR/WEE1 inhibitors and platinum, generating biomarker hypotheses for therapeutic responsiveness (Figure 5). PDCLs that are DDR deficient with high replication stress respond to both DDR targeting agents (eg, platinum and PARP inhibitors) and cell cycle checkpoint inhibitors (eg, ATR and WEE1 inhibitors), DDR-deficient PDCLs with low replication stress respond to DDR agents only, DDR-proficient PDCLs with high replication stress respond to cell cycle checkpoint inhibitors only, and DDR-proficient PDCLs with low replication stress respond to neither class of agent (Figure 5).

Potential Clinical Utility of the Replication Stress Signature

To assess the potential clinical validity and utility of these preclinical data, the relationship between the replication stress signature score and molecular subtypes in bulk tumor samples was assessed by using published transcriptomic data sets of PC.[5,9] This included whole transcriptome sequencing sets acquired through the ICGC totaling 94 patients with primary resected PC (Supplementary Figure 5). This recapitulated the association between squamous molecular subtype and high replication stress ($P = .006$) (Supplementary Figure 5), with 50% of squamous tumors in the top quartile of tumors ranked by the replication stress score.

The replication stress signature was then applied to The Cancer Genome Atlas[9] high epithelial cellularity set (ABSOLUTE purity ≥ 0.2), and the ICGC microarray transcriptomic data sets (Supplementary Figure 6). Again, the top-ranking quartile of replication stress signature was significantly enriched with squamous subtype PC (The Cancer Genome Atlas set, $P = .009$; microarray set, $P = .037$) (Supplementary Figure 6). We then examined the potential clinical utility of the replication stress signature in biopsy material acquired through the Precision-Panc endoscopic ultrasound fine-needle biopsy training cohort (n = 54), recruited and collected during the development of the Precision-Panc (Supplementary Figure 5*B*).[50] As in the other cohorts, this showed enrichment of the squamous subtype with high replication stress ($P = .027$) and provides proof-

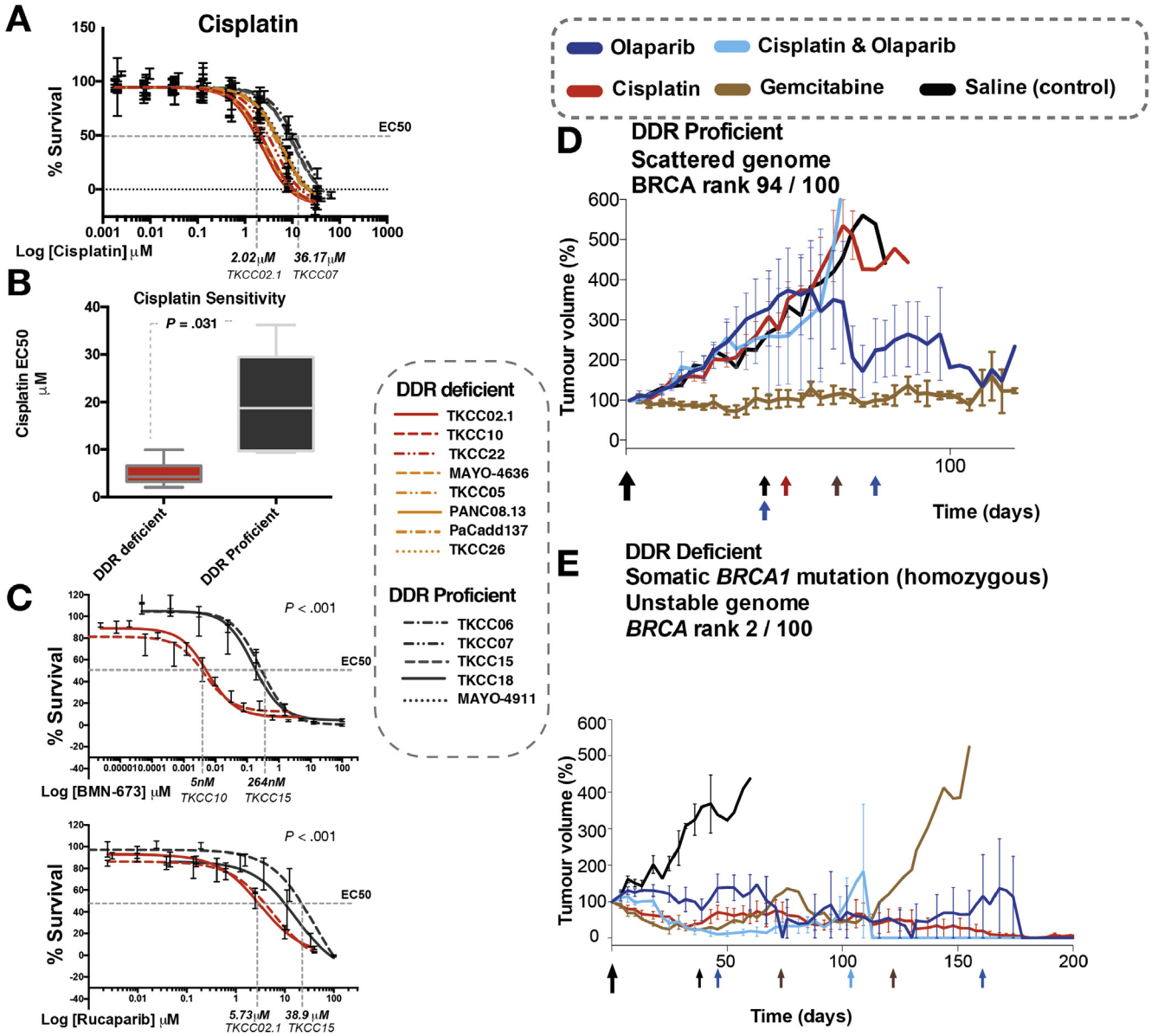

Figure 2. Targeting DDR-deficient PC with platinum and PARP inhibitors. (*A*) Cell viability after 72 hours of cisplatin treatment in PDCLs. The dotted line indicates that EC_{50} in the most sensitive PDCL was approximately 15 times more sensitive than the most resistant PDCLs. (*B*) Boxplot of mean cisplatin EC_{50} in PDCLS stratified by DDR status. The boxes represent the 95% confidence interval, and whiskers show the minimum and maximum range. *P* was calculated by using the Mann-Whitney test between the mean EC_{50} in each group. (*C*) PARP inhibitor (BMN-637 and rucaparib) response in PDCLs. The dotted lines indicate the EC_{50} between the most sensitive and most resistant PDCLs. *P* indicates the statistical difference between TKCC 10 (GPOL HRD test positive) and TKCC15 (DDR proficient) using nonlinear regression analysis. (*D*) PDX 2133 and (*E*) PDX 2179 (DDR deficient) treated with a panel of DNA-damaging agents and gemcitabine. The colored arrows indicate redosing of specific agents. M, mol/L.

of-principle clinical validity that the signature can be generated from fine-needle biopsy material and used as a putative biomarker in the clinical setting.

Discussion

Identifying responsive patient subgroups is crucial to therapeutic development and improving outcomes for PC. Genomic sequencing studies and the development of novel therapeutic agents has made DDR mechanisms one of the most attractive therapeutic opportunities in PC.[4,8] Using surrogate markers of DDR deficiency (GPOL HRD test, structural variation, the COSMIC BRCA mutational signature, and mutations in HR pathway genes) we show that DDR-deficient PCs respond preferentially to both platinum and PARP inhibitors in PDCLs (n = 15) and long-lasting complete and near-complete responses in a DDR-deficient PDX model with single-agent PARP inhibition with olaparib. This was as effective as cisplatin monotherapy or combination treatment with cisplatin and Olaparib,

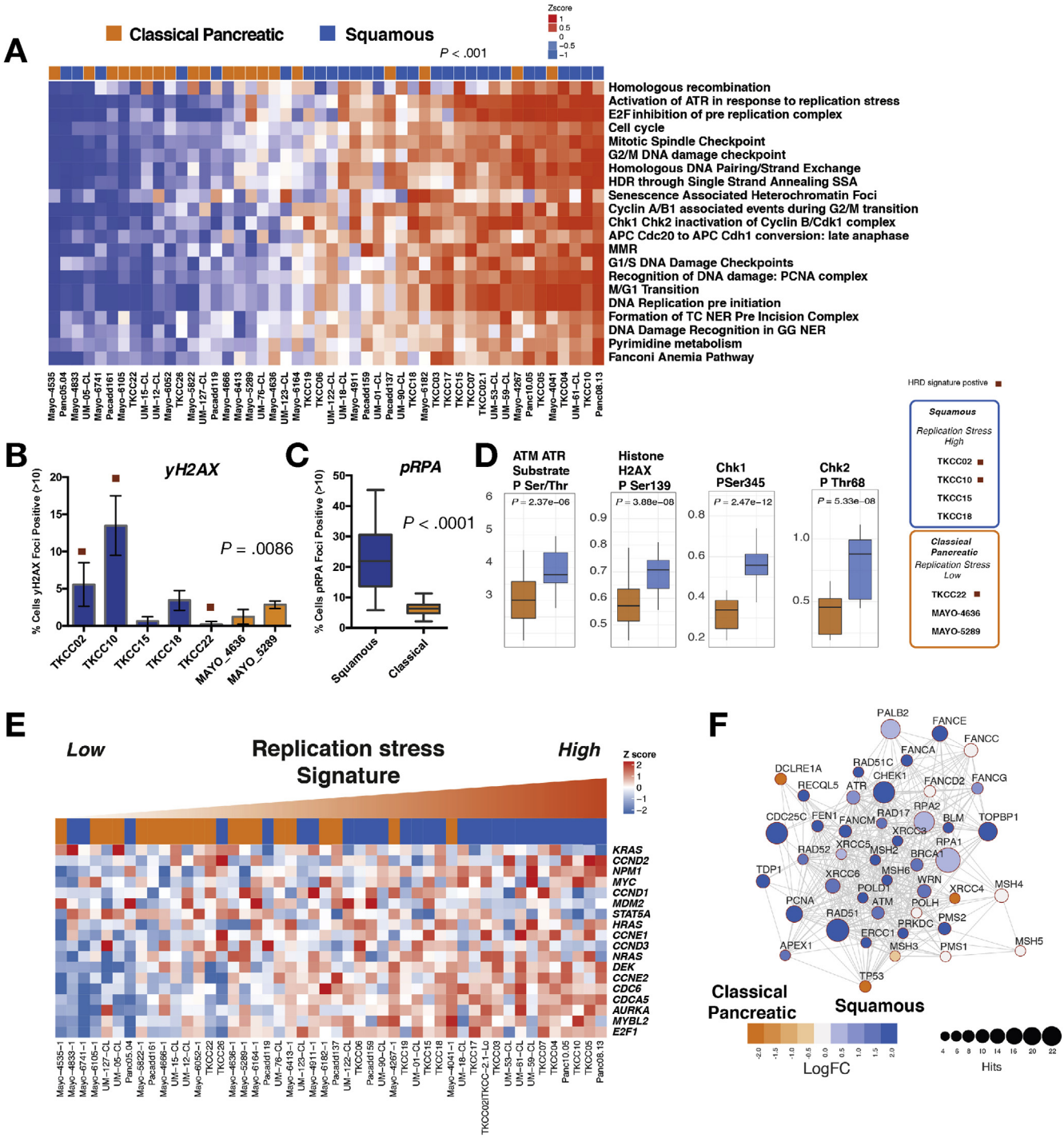

Figure 3. Replication stress in PDCLs of PC. (*A*) Heatmap of pathways and molecular processes (GO terms) involved in DNA maintenance and cell cycle regulation activated in replication stress and DNA damage response. PDCLs are ranked from right to left based on the decreasing novel transcriptomic signature score of replication stress, and molecular subtype is indicated in the top bar showing the association between activation of replication stress and the squamous subtype ($P < .001$, chi-square test, low vs high). (*B*, *C*) Immunofluorescent quantifications of (*B*) γH2AX and (*C*) pRPA at normal conditions are elevated in the squamous (*blue*) but not the classical pancreatic (*orange*) PDCLs. (*D*) Proteomic analysis using RPPA of a panel of PDCLs showed that replication stress response proteins are differentially activated in the squamous subtype. (*E*) Heatmap showing oncogene expression in PDCLs ranked from right to left by replication stress signature. Squamous PDCLs are enriched for oncogene activation and replication stress. (*F*) siRNA screening showing transcriptome functional interaction subnetwork, showing preferential dependencies of cell cycle control and DNA maintenance genes in the squamous subtype. Different node colors represent dependencies in different molecular subtypes, and the size of each node is relative to the number of siRNA hits. FC, fold change.

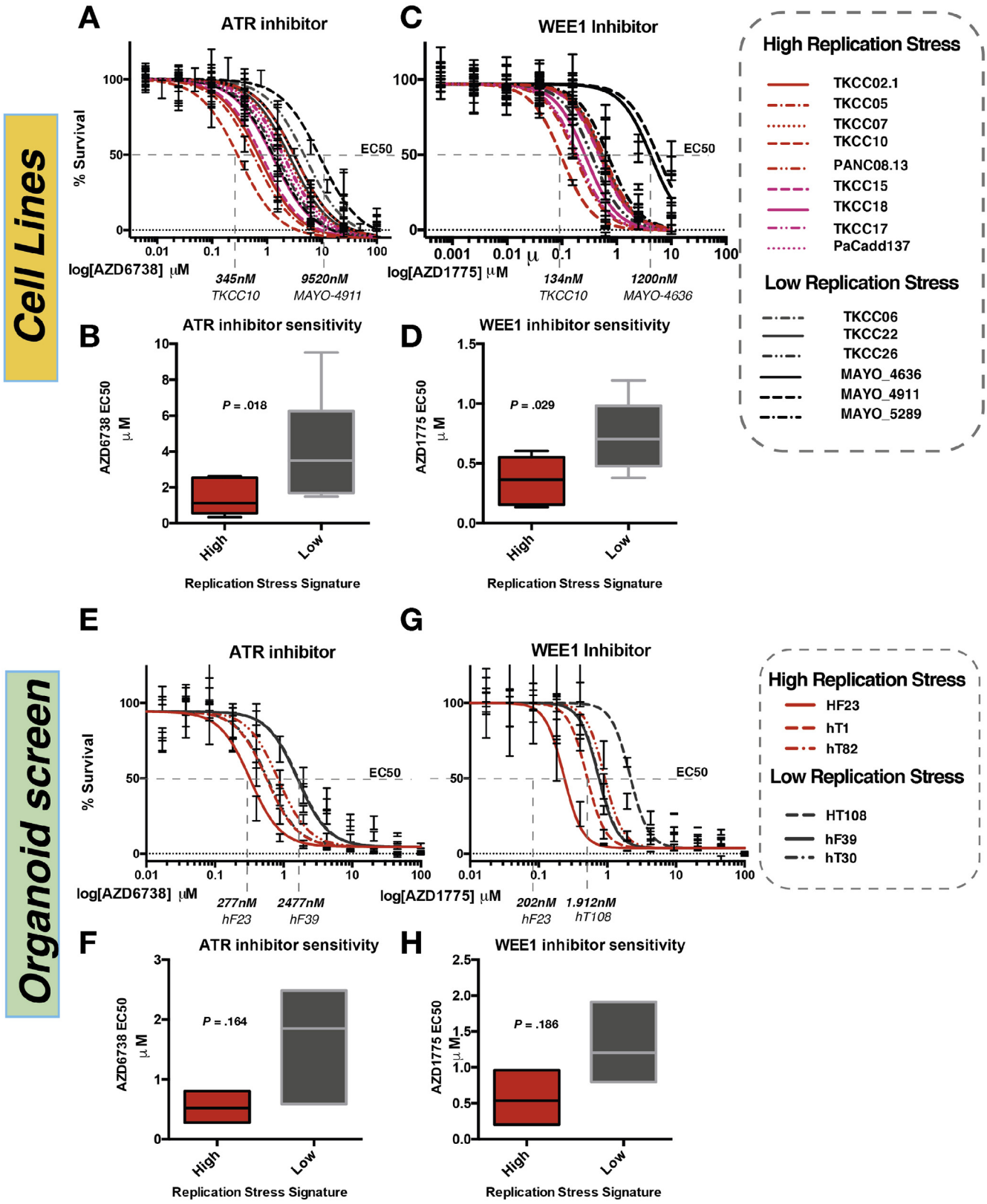

Figure 4. Targeting replication stress in PC. Dose response curves (EC_{50} shift) for (*A*) ATR and (*B*) WEE1 inhibitors calculated by using MTS assay in PDCLs after 72 hours of drug treatment. (*C*, *D*) Mean relative EC_{50} for PDCLs stratified by replication stress score. Patient-derived organoid drug screening dose response curves (EC_{50} shift) for (*E*) ATR and (*G*) WEE1 inhibitors calculated by using MTS assay after 72 hours of drug treatment. (*F*, *H*) Mean relative EC_{50} for PDCLs stratified by replication stress score. Each boxplot represents mean EC_{50}, and box and whiskers represent minimum and maximum EC_{50} with 95% confidence interval. *P* calculated by using Mann-Whitney test between mean EC_{50} in each group.

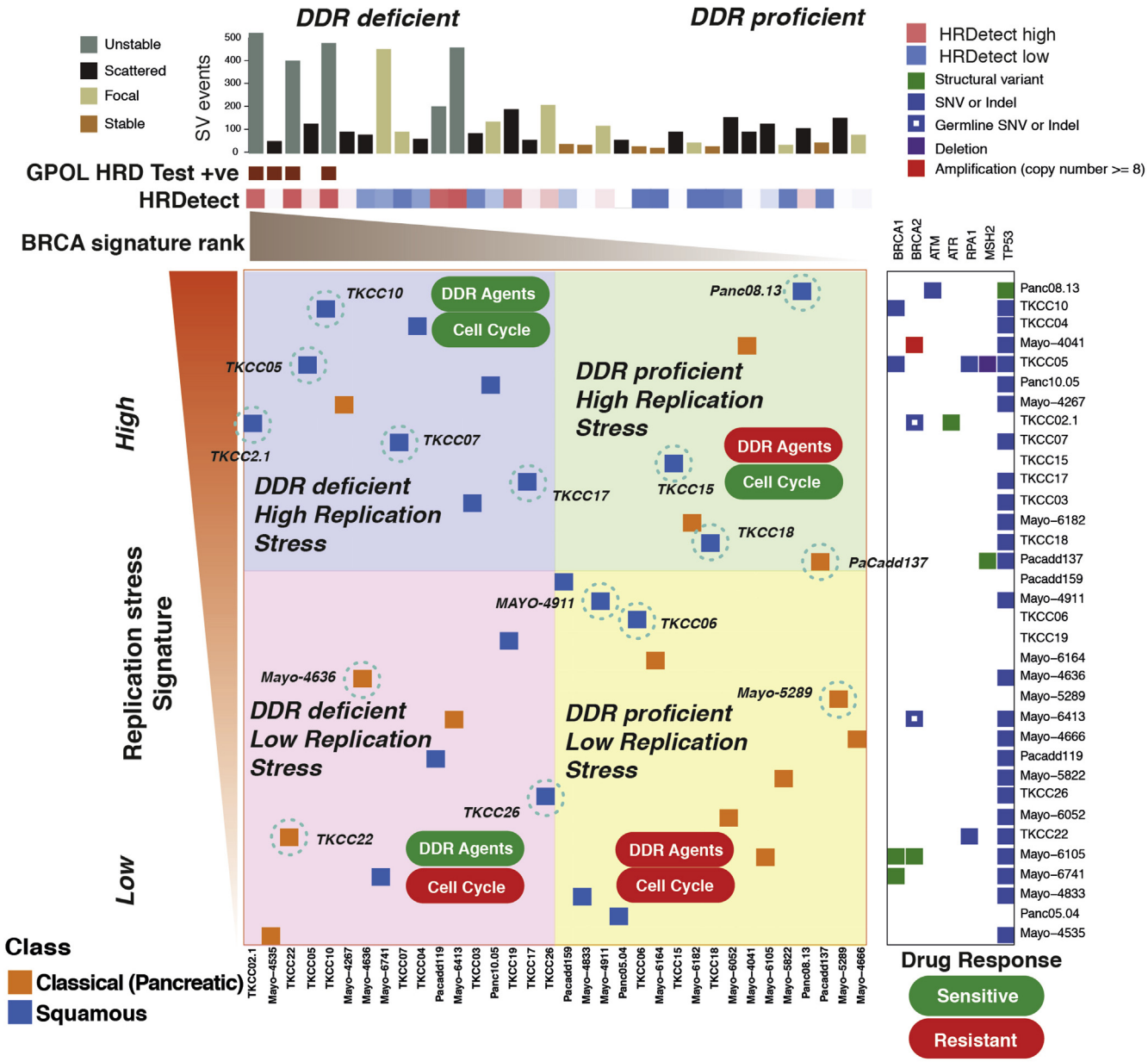

Figure 5. Relationship between DDR deficiency, replication stress, and therapeutic response in PDCLs of PC. PDCLs are ranked based on a novel transcriptomic signature of replication stress (*y*-axis) and a composite genomic readout of DDR deficiency (*x*-axis). DDR deficiency is a hierarchical score that incorporates the COSMIC BRCA mutational signature (signature 3), the number of structural variants distributed across the genome, and the GPOL HRD test associated with BRCA deficiency. Relative HRDetect score is indicated by colored scale. The combination of high/low states of each characteristic results in 4 groups. Squamous subtype PDCLs (*blue squares*) are associated with high replication stress ($P = .007$, chi-square test). PDCLs tested are identified and encircled in blue. DDR deficiency and the replication stress signature predicted differential therapeutic response.

suggesting that in appropriately selected patients, PARP inhibitor monotherapy can potentially induce clinically relevant responses similar to platinum. This provides potential therapeutic options for patients with poor performance status or after intolerance or acquired resistance to platinum has developed.[36] Predicting platinum response is more complex than using point mutations in DDR genes alone. In keeping with other studies,[51] biallelic loss-of-function mutations in HR genes, structural variation signatures, including >200 SVs,[4] and the GPOL HRD test appear to be robust, but they require testing in clinical settings. However, the COSMIC BRCA mutational signature is a poor predictor of platinum response in isolation. Selecting robust biomarkers for platinum response is crucial for clinical testing. The GPOL HRD test in conjunction with mutations in DDR genes has been selected as the biomarker of platinum response to investigate in PRIMUS-001 (ISRCTN75002153) and PRIMUS-002

(ISRCTN34129115), 2 phase 2/3 clinical trials on the Precision-Panc platform.

We define a novel replication stress signature which is associated with the squamous subtype in PDCLs and bulk tumors from multiple PC cohorts (n = 383 patients). Elevated replication stress, as defined by this signature, is associated with functional deficiencies in DNA replication, leading to a therapeutic vulnerability to novel agents as demonstrated by cell viability assays, organoid drug screenings, and siRNA functional screening. This molecular feature is independent of DDR status, platinum response, or molecular subtype. This suggests that molecular signatures, such as the replication stress signature, can be used as biomarkers for predicting response to ATR or WEE1 inhibitors and offer patients with DNA replication defects alternative therapeutic options to the standard-of-care platinum chemotherapy. Tumors that are DDR deficient can be targeted with platinum-based therapy or, in the context of a patient with reduced performance status or as the second line, PARP inhibitors. Patients with high replication stress can be targeted with ATR or WEE1 inhibitors, which can be combined with PARP inhibitors or platinum if concurrent DDR deficiency exists or after platinum resistance develops. This hypothesis will be tested in the PRIMUS-004 (ISRCTN16004234) clinical trial on the Precision-Panc platform, with the secondary endpoint of replication stress signature as a biomarker of response.

In summary, we developed and performed preclinical testing on novel biomarkers of DDR deficiency and replication stress that have potential clinical utility. Well-designed precision oncology platforms, such as Precision-Panc (precisionpanc.org), will enable biomarker-driven clinical testing and allow refinement of biomarkers predicting meaningful responses and potential translation into clinical practice.

Supplementary Material

Note: To access the supplementary material accompanying this article, visit the online version of *Gastroenterology* at www.gastrojournal.org, and at https://doi.org/10.1053/j.gastro.2020.09.043.

References

1. Siegel RL, Miller KD, Jemal A. Cancer statistics, 2019. CA Cancer J Clin 2019;69:7–34.
2. Rahib L, Smith BD, Aizenberg R, et al. Projecting cancer incidence and deaths to 2030: the unexpected burden of thyroid, liver, and pancreas cancers in the United States. Cancer Res 2014;74:2913–2921.
3. Biankin AV, Waddell N, Kassahn KS, et al. Pancreatic cancer genomes reveal aberrations in axon guidance pathway genes. Nature 2012;491(7424):399–405.
4. Waddell N, Pajic M, Patch AM, et al. Whole genomes redefine the mutational landscape of pancreatic cancer. Nature 2015;518(7540):495–501.
5. Bailey P, Chang DK, Nones K, et al. Genomic analyses identify molecular subtypes of pancreatic cancer. Nature 2016;531(7592):47–52.
6. Humphris JL, Patch AM, Nones K, et al. Hypermutation in pancreatic cancer. Gastroenterology 2017;152:68–74.
7. Witkiewicz AK, McMillan EA, Balaji U, et al. Whole-exome sequencing of pancreatic cancer defines genetic diversity and therapeutic targets. Nat Commun 2015;6:6744.
8. Dreyer SB, Chang DK, Bailey P, et al. Pancreatic cancer genomes: implications for clinical management and therapeutic development. Clin Cancer Res 2017;23:1638–1646.
9. The Cancer Genome Atlas Research Network. Integrated genomic characterization of pancreatic ductal adenocarcinoma. Cancer Cell 2017;32:185–203.
10. Notta F, Chan-Seng-Yue M, Lemire M, et al. A renewed model of pancreatic cancer evolution based on genomic rearrangement patterns. Nature 2016;538(7625):378–382.
11. **Jones S, Zhang X, Parsons DW**, et al. Core signaling pathways in human pancreatic cancers revealed by global genomic analyses. Science 2008;321(5897):1801–1806.
12. Biankin AV, Piantadosi S, Hollingsworth SJ. Patient-centric trials for therapeutic development in precision oncology. Nature 2015;526(7573):361–370.
13. Biankin AV, Maitra A. Subtyping pancreatic cancer. Cancer Cell 2015;28:411–413.
14. Collisson EA, Sadanandam A, Olson P, et al. Subtypes of pancreatic ductal adenocarcinoma and their differing responses to therapy. Nat Med 2011;17:500–503.
15. Connor AA, Denroche RE, Jang GH, et al. Association of distinct mutational signatures with correlates of increased immune activity in pancreatic ductal adenocarcinoma. JAMA Oncol 2017;3:774–783.
16. **Maurer C, Holmstrom SR, He J**, et al. Experimental microdissection enables functional harmonisation of pancreatic cancer subtypes. Gut 2019;68:1034–1043.
17. Puleo F, Nicolle R, Blum Y, et al. Stratification of pancreatic ductal adenocarcinomas based on tumor and microenvironment features. Gastroenterology 2018;155:1999–2013.
18. Moffitt RA, Marayati R, Flate EL, et al. Virtual microdissection identifies distinct tumor- and stroma-specific subtypes of pancreatic ductal adenocarcinoma. Nat Genet 2015;47:1168–1178.
19. Collisson EA, Bailey P, Chang DK, Biankin AV. Molecular subtypes of pancreatic cancer. Nat Rev Gastroenterol Hepatol 2019;16:207–220.
20. **Dreyer SB, Pinese M, Jamieson NB**, et al. Precision oncology in surgery: patient selection for operable pancreatic cancer. Ann Surg 2020;272:366–376.
21. Zhang J, Dai Q, Park D, et al. Targeting DNA replication stress for cancer therapy. Genes (Basel) 2016;7(8):51.
22. Lecona E, Fernandez-Capetillo O. Targeting ATR in cancer. Nat Rev Cancer 2018;18:586–595.
23. Hanahan D, Weinberg RA. Hallmarks of cancer: the next generation. Cell 2011;144:646–674.

24. Di Micco R, Fumagalli M, Cicalese A, et al. Oncogene-induced senescence is a DNA damage response triggered by DNA hyper-replication. Nature 2006;444(7119):638–642.
25. Macheret M, Halazonetis TD. Intragenic origins due to short G1 phases underlie oncogene-induced DNA replication stress. Nature 2018;555(7694):112–116.
26. Murphy JE, Wo JY, Ryan DP, et al. Total neoadjuvant therapy with FOLFIRINOX followed by individualized chemoradiotherapy for borderline resectable pancreatic adenocarcinoma: a phase 2 clinical trial. JAMA Oncol 2018;4:963–969.
27. Conroy T, Desseigne F, Ychou M, et al. FOLFIRINOX versus gemcitabine for metastatic pancreatic cancer. N Engl J Med 2011;364:1817–1825.
28. Conroy T, Hammel P, Hebbar M, et al. FOLFIRINOX or gemcitabine as adjuvant therapy for pancreatic cancer. N Engl J Med 2018;379:2395–2406.
29. Ruckert F, Aust D, Bohme I, et al. Five primary human pancreatic adenocarcinoma cell lines established by the outgrowth method. J Surg Res 2012;172:29–39.
30. Chou A, Froio D, Nagrial AM, et al. Tailored first-line and second-line CDK4-targeting treatment combinations in mouse models of pancreatic cancer. Gut 2018;67:2142–2155.
31. Pal K, Pletnev AA, Dutta SK, et al. Inhibition of endoglin-GIPC interaction inhibits pancreatic cancer cell growth. Mol Cancer Ther 2014;13:2264–2275.
32. Tiriac H, Belleau P, Engle DD, et al. Organoid profiling identifies common responders to chemotherapy in pancreatic cancer. Cancer Discov 2018;8:1112–1129.
33. **Nones K, Waddell N, Wayte N**, et al. Genomic catastrophes frequently arise in esophageal adenocarcinoma and drive tumorigenesis. Nat Commun 2014;5:5224.
34. **Patch AM, Christie EL, Etemadmoghadam D**, et al. Whole-genome characterization of chemoresistant ovarian cancer. Nature 2015;521(7553):489–494.
35. Davies H, Glodzik D, Morganella S, et al. HRDetect is a predictor of BRCA1 and BRCA2 deficiency based on mutational signatures. Nat Med 2017;23:517–525.
36. Golan T, Hammel P, Reni M, et al. Maintenance olaparib for germline *BRCA*-mutated metastatic pancreatic cancer. N Engl J Med 2019;381:317–327.
37. Shroff RT, Hendifar A, McWilliams RR, et al. Rucaparib monotherapy in patients with pancreatic cancer and a known deleterious *BRCA* mutation. JCO Precis Oncol 2018;2: PO.17.00316.
38. **McBride DJ, Etemadmoghadam D**, Cooke SL, et al. Tandem duplication of chromosomal segments is common in ovarian and breast cancer genomes. J Pathol 2012;227:446–455.
39. Ng CK, Cooke SL, Howe K, et al. The role of tandem duplicator phenotype in tumour evolution in high-grade serous ovarian cancer. J Pathol 2012;226:703–712.
40. Kotsantis P, Petermann E, Boulton SJ. Mechanisms of oncogene-induced replication stress: jigsaw falling into place. Cancer Discov 2018;8:537–555.
41. Karnitz LM, Zou L. Molecular pathways: targeting ATR in cancer therapy. Clin Cancer Res 2015;21:4780–4785.
42. **Zhang Y, Lai J**, Du Z, et al. Targeting radioresistant breast cancer cells by single agent CHK1 inhibitor via enhancing replication stress. Oncotarget 2016;7:34688–34702.
43. Zheng H, Shao F, Martin S, et al. WEE1 inhibition targets cell cycle checkpoints for triple negative breast cancers to overcome cisplatin resistance. Sci Rep 2017;7:43517.
44. Yap TA, Krebs MG, Postel-Vinay S, et al. Phase I modular study of AZD6738, a novel oral, potent and selective ataxia telangiectasia Rad3-related (ATR) inhibitor in combination (combo) with carboplatin, olaparib or durvalumab in patients (pts) with advanced cancers. Eur J Cancer 2018;69(Suppl 1):S2.
45. Do K, Wilsker D, Ji J, et al. Phase I study of single-agent AZD1775 (MK-1775), a Wee1 kinase inhibitor, in patients with refractory solid tumors. J Clin Oncol 2015;33:3409–3415.
46. Dillon MT, Boylan Z, Smith D, et al. PATRIOT: a phase I study to assess the tolerability, safety and biological effects of a specific ataxia telangiectasia and Rad3-related (ATR) inhibitor (AZD6738) as a single agent and in combination with palliative radiation therapy in patients with solid tumours. Clin Transl Radiat Oncol 2018;12:16–20.
47. Krebs M, Lopez J, El-Khoueiry L, et al. Phase I clinical and translational evaluation of AZD6738 in combination with durvalumab in patients (pts) with lung or head and neck carcinoma. Ann Oncol 2018;29(Suppl 8):VIII135.
48. Leijen S, van Geel RM, Sonke GS, et al. Phase II study of WEE1 inhibitor AZD1775 plus carboplatin in patients with TP53-mutated ovarian cancer refractory or resistant to first-line therapy within 3 months. J Clin Oncol 2016;34:4354–4361.
49. Leijen S, van Geel RM, Pavlick AC, et al. Phase I study evaluating WEE1 inhibitor AZD1775 as monotherapy and in combination with gemcitabine, cisplatin, or carboplatin in patients with advanced solid tumors. J Clin Oncol 2016;34:4371–4380.
50. Dreyer SB, Jamieson NB, Evers L, et al. Feasibility and clinical utility of endoscopic ultrasound guided biopsy of pancreatic cancer for next-generation molecular profiling. Chin Clin Oncol 2019;8(2):16.
51. Park W, Chen J, Chou JF, et al. Genomic methods identify homologous recombination deficiency in pancreas adenocarcinoma and optimize treatment selection. Clin Cancer Res 2020;26:3239–3247.

Author names in bold designate shared co-first authorship.

Received August 8, 2019. Accepted September 28, 2020.

Correspondence
Address correspondence to: David K. Chang, MD, PhD, Wolfson Wohl Cancer Research Centre, Institute of Cancer Sciences, University of Glasgow, Garscube Estate, Switchback Road, Bearsden, Glasgow, Scotland G61 1BD, United Kingdom. e-mail: david.chang@glasgow.ac.uk; fax: +44 141 330 5834; or Andrew V Biankin, MD, PhD, Wolfson Wohl Cancer Research Centre, Institute of Cancer Sciences, University of Glasgow, Garscube Estate, Switchback Road, Bearsden, Glasgow, Scotland G61 1BD, United Kingdom. e-mail: andrew.biankin@glasgow.ac.uk; fax: +44 141 330 5834.

Acknowledgments
Glasgow Precision Oncology Laboratory

Sarah Allison,[1] Peter J. Bailey,[1] Ulla-Maja Bailey,[1] Andrew V. Biankin,[1] Dario Beraldi,[1] Holly Brunton,[1] Giuseppina Caligiuri,[1] Euan Cameron,[1] David K. Chang,[1,2] Susanna L. Cooke,[1] Richard Cunningham,[1] Stephan Dreyer,[1,2] Paul Grimwood,[1] Shane Kelly,[1] Eirini-Maria Lampraki,[1] John Marshall,[1] Sancha Martin,[1] Brian McDade,[1] Daniel McElroy,[1] Elizabeth A. Musgrove,[1] Craig Nourse,[1] Viola Paulus-Hock,[1] Donna Ramsay,[1] Rosie Upstill-Goddard,[1] Derek Wright,[1] Marc D. Jones,[1] Lisa Evers,[1] Selma Rebus,[1] Lola Rahib,[1] Bryan Serrels,[1] Jane Hair,[1] Nigel B. Jamieson,[1,2] Colin J. McKay,[1,2] Paul Westwood,[1,4] Nicola Williams,[1,4] and Fraser Duthie[1,3]

[1]Glasgow Precision Oncology Laboratory, University of Glasgow, Institute of Cancer Sciences, Wolfson Wohl Cancer Research Centre, Glasgow, United Kingdom; [2]West of Scotland Pancreatic Unit, Glasgow Royal Infirmary, Glasgow, United Kingdom; [3]Department of Pathology, Southern General Hospital, Greater Glasgow and Clyde National Health Service, Glasgow, United Kingdom; [4]West of Scotland Genetic Services, National Health Service, Greater Glasgow and Clyde, Queen Elizabeth University Hospital Campus, Glasgow, United Kingdom.

Australian Pancreatic Cancer Genome Initiative

Garvan Institute of Medical Research: Andrew V. Biankin,[1,2] Amber L. Johns,[1] Amanda Mawson,[1] David K. Chang,[1,2] Christopher J. Scarlett,[1] Mary-Anne L. Brancato,[1] Sarah J. Rowe,[1] Skye H. Simpson,[1] Mona Martyn-Smith,[1] Michelle T. Thomas,[1] Lorraine A. Chantrill,[1] Venessa T. Chin,[1] Angela Chou,[1] Mark J. Cowley,[1] Jeremy L. Humphris,[1] Marc D. Jones,[1,2] R. Scott Mead,[1] Adnan M. Nagrial,[1] Marina Pajic,[1] Jessica Pettit,[1] Mark Pinese,[1] Ilse Rooman,[1] Jianmin Wu,[1] Jiang Tao,[1] Renee DiPietro,[1] Clare Watson,[1] Angela Steinmann,[1] Hong Ching Lee,[1] Rachel Wong,[1] Andreia V. Pinho,[1] Marc Giry-Laterriere,[1] Roger J. Daly,[1] Elizabeth A. Musgrove,[1,2] and Robert L. Sutherland.[1] Queensland Centre for Medical Genomics / Institute for Molecular Biosciences: Sean M. Grimmond,[3] Nicola Waddell,[3] Karin S. Kassahn,[3] David K. Miller,[3] Peter J. Wilson,[3] Ann-Marie Patch,[3] Sarah Song,[3] Ivon Harliwong,[3] Senel Idrisoglu,[3] Craig Nourse,[3] Ehsan Nourbakhsh,[3] Suzanne Manning,[3] Shivangi Wani,[3] Milena Gongora,[3] Matthew Anderson,[3] Oliver Holmes,[3] Conrad Leonard,[3] Darrin Taylor,[3] Scott Wood,[3] Christina Xu,[3] Katia Nones,[3] J. Lynn Fink,[3] Angelika Christ,[3] Tim Bruxner,[3] Nicole Cloonan,[3] Felicity Newell,[3] John V. Pearson,[3] Peter Bailey,[3] Michael Quinn,[3] Shivashankar Nagaraj,[3] Stephen Kazakoff,[3] Nick Waddell,[3] Keerthana Krisnan,[3] Kelly Quek,[3] and David Wood.[3] Royal North Shore Hospital: Jaswinder S. Samra,[4] Anthony J. Gill,[4] Nick Pavlakis,[4] Alex Guminski,[4] Christopher Toon.[4] Bankstown Hospital: Ray Asghari,[5] Neil D. Merrett,[5] Darren Pavey,[5] and Amitabha Das.[5] Liverpool Hospital: Peter H. Cosman,[6] Kasim Ismail,[6] and Chelsie O'Connnor.[6] Westmead Hospital: Vincent W. Lam,[7] Duncan McLeod,[7] Henry C. Pleass,[7] Arthur Richardson,[7] and Virginia James.[7] Royal Prince Alfred Hospital: James G. Kench,[8] Caroline L. Cooper,[8] David Joseph,[8] Charbel Sandroussi,[8] Michael Crawford,[8] James Gallagher.[8] Fremantle Hospital: Michael Texler,[9] Cindy Forest,[9] Andrew Laycock,[9] Krishna P. Epari,[9] Mo Ballal,[9] David R. Fletcher,[9] and Sanjay Mukhedkar.[9] Sir Charles Gairdner Hospital: Nigel A. Spry,[10] Bastiaan DeBoer,[10] Ming Chai.[10] St John of God Healthcare: Nikolajs Zeps,[11] Maria Beilin,[11] and Kynan Feeney.[11] Royal Adelaide Hospital: Nan Q. Nguyen,[12] Andrew R. Ruszkiewicz,[12] Chris Worthley,[12] Chuan P. Tan,[12] and Tamara Debrencini.[12] Flinders Medical Centre: John Chen,[13] Mark E. Brooke-Smith,[13] and Virginia Papangelis.[13] Greenslopes Private Hospital: Henry Tang,[14] and Andrew P. Barbour.[14] Envoi Pathology: Andrew D. Clouston,[15] and Patrick Martin.[15] Princess Alexandria Hospital: Thomas J O'Rourke,[16] Amy Chiang,[16] Jonathan W. Fawcett,[16] Kellee Slater,[16] Shinn Yeung,[16] Michael Hatzifotis,[16] and Peter Hodgkinson.[16] Austin Hospital: Christopher Christophi,[17] Mehrdad Nikfarjam,[17] and Angela Mountain.[17] Victorian Cancer Biobank.[18] Johns Hopkins Medical Institutes: James R. Eshleman,[19] Ralph H. Hruban,[19] Anirban Maitra,[19] Christine A. Iacobuzio-Donahue,[19] Richard D. Schulick,[19] Christopher L. Wolfgang,[19] Richard A. Morgan,[19] and Mary Hodgin.[19] ARC-Net Centre for Applied Research on Cancer: Aldo Scarpa,[20] Rita T. Lawlor,[20] Stefania Beghelli,[20] Vincenzo Corbo,[20] Maria Scardoni,[20] and Claudio Bassi.[20] University of California, San Francisco: Margaret A. Tempero.[21] University of Glasgow: Andrew V. Biankin,[1,2,22] Sean M. Grimmond,[2,3] David K. Chang,[1,2,22] Elizabeth A. Musgrove,[2] Marc D. Jones,[1,2] Craig Nourse,[2,3] Nigel B. Jamieson,[2,22] and Janet S. Graham.[2,22] Greater Glasgow and Clyde National Health Service: Andrew V. Biankin[1,2,22] David K. Chang,[1,2,22] Nigel B. Jamieson,[2,22] and Janet S. Graham.[2,22]

[1]The Kinghorn Cancer Centre, Garvan Institute of Medical Research, 370 Victoria Street, Darlinghurst, Sydney, New South Wales, Australia; [2]Wolfson Wohl Cancer Research Centre, Institute of Cancer Sciences, University of Glasgow, Glasgow, Scotland, United Kingdom; [3]Queensland Centre for Medical Genomics, Institute for Molecular Bioscience, University of Queensland, St Lucia, Queensland, Australia; [4]Royal North Shore Hospital, St Leonards, New South Wales, Australia; [5]Bankstown Hospital, Bankstown, New South Wales, Australia; [6]Liverpool Hospital, Liverpool, New South Wales, Australia; [7]Westmead Hospital, Westmead, New South Wales, Australia; [8]Royal Prince Alfred Hospital, Camperdown, New South Wales, Australia; [9]Fremantle Hospital, Fremantle, Western Australia, Australia; [10]Sir Charles Gairdner Hospital, Nedlands, Western Australia, Australia; [11]St John of God Healthcare, Subiaco, Western Australia, Australia; [12]Royal Adelaide Hospital, Adelaide, South Australia, Australia; [13]Flinders Medical Centre, Bedford Park, South Australia, Australia; [14]Greenslopes Private Hospital, Greenslopes, Queensland, Australia; [15]Envoi Pathology, Herston, Queensland, Australia; [16]Princess Alexandria Hospital, Woolloongabba, Queensland, Australia; [17]Austin Hospital, Heidelberg, Victoria, Australia; [18]Victorian Cancer Biobank, Carlton, Victoria, Australia; [19]Johns Hopkins Medical Institute, Baltimore, Maryland; [20]ARC-NET Center for Applied Research on Cancer, University of Verona, Verona, Italy; [21]University of California, San Francisco, San Francisco, California; and [22]Greater Glasgow and Clyde National Health Service, Glasgow, United Kingdom.

CRediT Authorship Contributions

Stephan B. Dreyer, MD, PhD (Conceptualization: Lead; Data curation: Lead; Formal analysis: Lead; Funding acquisition: Equal; Investigation: Lead; Methodology: Lead; Project administration: Equal; Validation: Equal; Visualization: Equal; Writing – original draft: Lead; Writing – review & editing: Lead); Rosie Upstill-Goddard, PhD (Formal analysis: Equal; Investigation: Equal; Software: Equal; Visualization: Equal); Viola Paulus-Hock, BSc (Data curation: Supporting); Clara Paris, BSc (Data curation: Supporting; Investigation: Supporting); Eirini-Maria Lampraki, PhD (Data curation: Supporting; Investigation: Supporting); Eloise Dray, PhD (Data curation: Supporting; Formal analysis: Supporting; Investigation: Supporting; Methodology: Supporting; Supervision: Supporting); Bryan Serrels, PhD (Data curation: Supporting; Methodology: Supporting); Giuseppina Caligiuri, BSc (Data curation: Supporting); Selma Rebus, MSc (Data curation: Supporting; Resources: Supporting); Dennis Plenker, PhD (Data curation: Supporting); Zachary Galluzzo, BSc (Data curation: Supporting); Holly Brunton, PhD (Data curation: Supporting); Richard Cunningham, BSc (Data curation: Supporting); Mathias Tesson, PhD (Data curation: Supporting); Craig Nourse, PhD (Data curation: Supporting); Ulla-Maja Bailey, PhD (Data curation: Supporting); Marc Jones, MSc (Data curation: Supporting); Kim Moran-Jones, PhD (Data curation: Supporting); Derek W. Wright, BSc (Data curation: Supporting; Formal analysis: Supporting); Fraser Duthie, MBChB, PhD (Data curation: Supporting); Karin Oien, MBChB, PhD (Data curation: Supporting); Lisa Evers, BSc (Data curation: Supporting); Colin J. McKay, MBChB, MD (Data curation: Supporting); Grant A. McGregor, PhD (Data curation: Supporting); Aditi Gulati, PhD (Data curation: Supporting); Rachel Brough, PhD (Data curation: Supporting); Ilirjana Bajrami, PhD (Data curation: Supporting); Stephan Pettitt, PhD (Data curation: Supporting); Michele L. Dziubinski, PhD (Data curation: Supporting); Juliana Candido, PhD (Data curation: Supporting); Frances Balkwill, PhD (Data curation: Supporting); Simon T. Barry, PhD (Data curation: Supporting; Resources: Supporting); Robert Grützmann, MD (Resources: Supporting); Lola Rahib, BSc (Data curation: Supporting); Amber Johns, BMedSc (Data curation: Equal; Funding acquisition: Supporting; Project administration: Supporting; Resources: Supporting); Marina Pajic, PhD (Data curation: Supporting; Resources: Supporting); Fieke E.M. Froeling, MD, PhD (Investigation: Supporting; Methodology: Supporting; Resources: Supporting); Philip Beer, MBChB, PhD (Formal analysis: Supporting; Investigation: Supporting); Elizabeth A. Musgrove, PhD (Conceptualization: Supporting; Funding acquisition: Equal; Project administration: Equal; Resources: Equal); Gloria M. Petersen, PhD (Data curation: Supporting); Alan Ashworth, MD, PhD (Data curation: Supporting; Resources: Supporting); Margaret C. Frame, PhD (Resources: Supporting); Howard C. Crawford, PhD (Resources: Supporting); Diane M. Simeone, MD, PhD (Resources: Supporting); Chris Lord, PhD (Conceptualization: Supporting; Resources: Supporting); Debabrata Mukhopadhyay, PhD (Resources: Supporting); Christian Pilarsky, PhD (Resources: Supporting); David Tuveson, PhD (Resources: Supporting; Validation: Supporting); Susanna L. Cooke, PhD (Data curation: Supporting; Formal analysis: Supporting; Funding acquisition: Equal; Resources: Supporting; Software: Equal); Nigel B. Jamieson, MD, PhD (Conceptualization: Supporting; Data curation: Supporting; Funding acquisition: Supporting; Investigation: Supporting; Methodology: Supporting; Writing – original draft: Supporting; Writing – review & editing: Supporting); Jennifer P. Morton, PhD (Data curation: Supporting); Owen J. Sansom, PhD (Data curation: Supporting; Funding acquisition: Equal; Resources: Equal); Peter J. Bailey, PhD (Data curation: Equal; Formal analysis: Equal; Investigation: Supporting; Methodology: Supporting; Resources: Supporting; Software: Equal; Visualization: Supporting); Andrew V. Biankin, MD, PhD (Conceptualization: Equal; Data curation: Equal; Formal analysis: Equal; Funding acquisition: Lead; Investigation: Equal; Methodology: Equal; Project administration: Equal; Resources: Equal; Software: Equal; Supervision: Equal; Validation: Equal; Visualization: Equal; Writing – original draft: Equal; Writing – review & editing: Equal); David K. Chang, PhD (Conceptualization: Equal; Data curation: Equal; Formal analysis: Equal; Funding acquisition: Equal; Investigation: Equal; Methodology: Equal; Project administration: Equal; Resources: Equal; Software: Equal; Supervision: Equal; Validation: Equal; Visualization: Equal; Writing – original draft: Equal; Writing – review & editing: Equal).

Conflicts of interest
This author discloses the following: Simon T. Barry is a senior principal scientist at AstraZeneca. The remaining authors disclose no conflicts.

Funding
This work was supported by the National Health and Medical Research Council of Australia (631701, 535903, 427601); Queensland Government National and International Research Alliances Program (NIRAP); University of Queensland; Institute for Molecular Bioscience; Australian Government: Department of Innovation, Industry, Science and Research; Australian Cancer Research Foundation; Cancer Council New South Wales (NSW) (SRP06-01, SRP11-01.ICGC); Cancer Institute NSW (10/ECF/2-26, 06/ECF/1-24, 09/CDF/2-40, 07/CDF/1-03, 10/CRF/1-01, 08/RSA/1-15, 07/CDF/1-28, 10/CDF/2-26,10/FRL/2-03, 06/RSA/1-05, 09/RIG/1-02, 10/TPG/1-04, 11/REG/1-10, 11/CDF/3-26); Garvan Institute of Medical Research; Avner Nahmani Pancreatic Cancer Research Foundation; R.T. Hall Trust; Petre Foundation; Philip Hemstritch Foundation; Gastroenterological Society of Australia; American Association for Cancer Research; Landon Foundation–INNOVATOR Award; Royal Australasian College of Surgeons; Royal Australasian College of Physicians; Royal College of Pathologists of Australasia; Susan Wojcicki and Dennis Tropper; National Institutes of Health grants CA62924, 5R01CA150190-07, and P50 CA102701; Cancer Research UK C29717/A17263, C29717/A18484, C596/A18076, C596/A20921, and A23526; Wellcome Trust Senior Investigator Award 103721/Z/14/Z; Pancreatic Cancer UK Future Research Leaders Fund FLF2015_04_Glasgow; Scottish Genome Partnership SEHHD-CSO 1175759/2158447; MRC/EPSRC Glasgow Molecular Pathology Node; The Howat Foundation; Italian Cancer Genome Project–Ministry of University (FIRB RBAP10AHJB); Associazione Italiana Ricerca Cancro (grant no. 12182); FP7 European Community Grant Cam-Pac (no. 602783); Italian Ministry of Health (FIMP- CUP_J33G13000210001); and International Cancer Genome Consortium, Ontario Institute for Cancer Research.

Supplementary Materials and Methods

Australian Pancreatic Cancer Genome Initiative

Sydney South West Area Health Service Human Research Ethics Committee, western zone (protocol number 2006/54); Sydney Local Health District Human Research Ethics Committee (X11-0220); Northern Sydney Central Coast Health Harbour Human Research Ethics Committee (0612-251M); Royal Adelaide Hospital Human Research Ethics Committee (091107a); Metro South Human Research Ethics Committee (09/ QPAH/220); South Metropolitan Area Health Service Human Research Ethics Committee (09/324); Southern Adelaide Health Service/Flinders University Human Research Ethics Committee (167/10); Sydney West Area Health Service Human Research Ethics Committee (Westmead campus) (HREC2002/3/4.19); The University of Queensland Medical Research Ethics Committee (2009000745); Greenslopes Private Hospital Ethics Committee (09/34); North Shore Private Hospital Ethics Committee. Johns Hopkins medical institutions: Johns Hopkins Medicine institutional review board (NA00026689). Ethikkommission an der Technischen Universität Dresden (approval numbers EK30412207 and EK357112012). University of Michigan institutional review board (HUM00025339). Mayo Clinic institutional review board (no. 66-06)

PRECISION-Panc Endoscopic Ultrasound Training Cohort

Ethical approval was obtained for collecting additional research biopsy samples from patients undergoing endoscopic ultrasound-guided biopsies for investigation of possible PC (ethical approval number: 17/WS/0085). Fully informed consent was obtained for all patients from whom additional biopsy samples were taken. Samples were anonymized at the point of collection, with only the PhD candidate being able to identify patients from research samples.

Whole-Genome Library Preparation

Whole-genome libraries were generated by using either the Illumina TruSeq DNA LT sample preparation kit (part nos. FC-121–2001 and FC-121–2001) or the Illumina TruSeq DNA PCR-Free LT sample preparation kit (part nos. FC-121–3001 and FC-121–3002) according to the manufacturer's protocols with some modifications (Illumina, part nos. 15026486 Rev. C July 2012 and 15036187 Rev. A January 2013 for the 2 different kits, respectively). For the TruSeq DNA LT sample preparation kit, 1 μg of genomic DNA was used as input for fragmentation to approximately 300 base pairs (bp), followed by an Solid Phase Reversible Immobilization (SPRI)-bead cleanup with the AxyPrep Mag PCR Clean-Up kit (Corning, part no. MAG-PCR-CL-250). After end repair, 3′ adenylation, and adaptor ligation, the libraries were size-selected by using a double SPRI-bead method to obtain libraries with an insert size of approximately 300 bp. The size-selected libraries were subjected to 8 cycles of polymerase chain reaction (PCR) to produce the final whole-genome libraries ready for sequencing. For the TruSeq DNA PCR-Free LT sample preparation kit, 1 μg of genomic DNA was used as input for fragmentation to approximately 350 bp, followed by an end-repair step and then a size selection using the double SPRI-bead method to obtain libraries with an insert size of approximately 350 bp. The size-selected libraries then underwent 3′ adenylation and adaptor ligation to produce final whole genome libraries ready for sequencing. Before sequencing, whole-genome libraries were qualified via the Agilent (Santa Clara, CA) BioAnalyzer 2100 with the High Sensitivity DNA Kit (Agilent, part no. 5067-4626). Quantification of libraries for clustering was performed using the KAPA Library Quantification Kit–Illumina/ Universal (KAPA Biosystems, part no. KK4824) in combination with the Life Technologies Viia 7 real-time PCR instrument.

RNA-Sequencing Library Generation and Sequencing

RNA-seq libraries were generated by using TruSeq Stranded Total RNA (part no. 15031048 Rev. D April 2013) kits on a PerkinElmer Sciclone G3 NGS Workstation (product no. SG3- 31020-0300). Ribosomal depletion step was performed on 1 μg of total RNA by using Ribo-Zero Gold before a heat fragmentation step aimed at producing libraries with an insert size between 120 and 200 bp. Complementary DNA was then synthesized from the enriched and fragmented RNA by using Invitrogen (San Diego, CA) SuperScript II Reverse Transcriptase (catalog no. 18064) and random primers. The resulting cDNA was further converted into double-stranded DNA in the presence of deoxyuridine triphosphate to prevent subsequent amplification of the second strand and thus maintain the strandedness of the library. After 3′ adenylation and adaptor ligation, libraries were subjected to 15 cycles of PCR to produce RNAseq libraries ready for sequencing. Before sequencing, exome and RNAseq libraries were qualified and quantified via the Caliper LabChip GX (part no. 122000; East Lyme, CT) instrument using the DNA High Sensitivity Reagent kit (product no. CLS760672). Quantification of libraries for clustering was performed with the KAPA Library Quantification Kits for Illumina sequencing platforms (kit code KK4824) in combination with Life Technologies Viia 7 real-time PCR instrument.

Weighted Gene Coexpression Network Analysis

Weighted gene coexpression network analysis (WGCNA) was used to generate a transcriptional network from rlog-normalized RNAseq data.[1] Briefly, WGCNA clusters genes into network modules by using a TOM. The TOM is a highly robust measure of network interconnectedness and essentially provides a measure of the connection strength between 2 adjacent genes and all other genes in a network. Genes are clustered by using 1 – TOM as the distance measure, and gene modules are defined as branches of the resulting cluster tree using a dynamic branch-cutting algorithm.

The module eigengene is used as a measure of module expression in a given sample and is defined as the first principal component of a module. To relate sample traits of interest to gene modules, sample traits were correlated to module eigengenes, and significance was determined by a Student asymptotic P value for the given correlations. To relate gene modules to PDCL subtypes, module eigengenes were stratified by subtype, and subtype significance was determined by the Kruskal-Wallis test.

Module preservation as implemented in WGCNA detects the conservation of gene pairs between 2 networks (eg, PDCL and bulk). Two composite measures were used to assess module preservation, namely, median rank and $Z_{summary}$. Median rank was used to identify module preservation, and $Z_{summary}$ was used to assess the significance of module preservation via permutation testing. Permutation was performed 200 times; modules with a $Z_{summary}$ score of >10 indicate preservation, 2–10 indicates weak to moderate preservation, and <2 indicates no preservation in the permutations.

Reverse Phase Protein Array. Samples were lysed in RIPA lysis buffer (50mM Tris-HCL at pH7.4, 150mM Sodium Chloride, 5mM EGTA, 0.1% SDS, 1% NP40, 1% Deoxycholate, supplemented protease and phosphatase inhibitor tablets; Roche Applied Science Cat. #: 05056489001 and 04906837001) for 30 min on ice and cleared by centrifugation at 14K for 15 min at 4°C. Protein concentration was determined using a Bradford assay (Sigma) and all samples were normalized to 2mg/ml. 4x SDS sample buffer (40% Glycerol, 8% SDS, 0.25M Tris-HCL, pH 6.8. 1/10th vol/vol 2-mercaptoethanol) was added to each sample, followed by incubation at 80°C for 5 mins. Serial dilutions (1, 0.5, 0.25, 0.125) were then prepared by diluting samples in PBS. Samples were printed onto Avid nitrocellulose coated glass slides (Grace Biolabs) using an Aushon 2470 microarrayer (Aushon Biosystems), with 2 technical replicates per sample. Slides were processed as follows: 4 x 15 min washes with dH20, incubated with antigen retrieval agent (Reblot strong, Millipore) for 15 min, 3 x 5 min washes with PBST, incubated with superblock TBST (ThermoFisher Scientific) for 10 min, 3 x 5 min washes with TBST, incubated with primary antibodies (all 1:200) diluted in superblock TBST for 60 mins, 3 x 5 min washes with TBST, blocked with superblock TBST for 10 mins, 3 x 5 min washes with TBST, incubated with anti-rabbit dylight 800 secondary Ab (1:2000 in superblock TBST)(Cell Signalling Technologies) for 30 mins, 3 x 5 min washes with TBST, 1 x 5 min wash with dH20, slides spun at 2000rpm for 5mins and allowed to air dry in the dark. An additional slide was stained with FAST Green FCF for normalization against total protein: 3 x 5min washes with dH20, incubated for 15 mins in 1% NaOH, slides rinsed 20 x in dH20, incubated for 10 min in dH20, incubated in de-stain (30% methanol, 7% glacial acetic acid, 63% dH20) for 15 min, incubated for 3 mins in FAST green staining solution (0.0025%w/v FAST green in de-stain), rinsed 20 x in dH20, incubated for 15 mins in de-stain solution, rinsed 20 x in dH20, spun at 2000rpm for 5 mins and allowed to air dry in the dark. All steps were performed at room temperature with agitation. Slides were visualized using an Innopsys 710AL infra-red microarray scanner and signals quantified using MAPIX microarray image analysis software (Innopsys). Non-specific signals were determined by omitting the primary antibody incubation step. All signals were within the linear range of detection with an R2 value >0.9. Final output is the median value for each dilution series as fentogram, background subtracted and normalized for protein loading.

Small Interfering RNA Screening

Before siRNA screening, the optimal cell number per well and optimal reverse transfection reagents for each PDCL were identified by assessing transfection efficiency using 6 different transfection reagents (Dharmafect 1-4, RNAimax, Lipofectamine 2000; Invitrogen, ThermoFisher), based on the manufacturers' instructions. Experimental conditions were selected that met the following criteria: (1) compared to a mock control (no lipid, no siRNA), the transfection of nonsilencing negative control siRNA caused no more than 20% cell inhibition; (2) compared to nonsilencing negative control siRNA, the transfection of PLK1–targeting siRNA caused more than 80% cell inhibition; and (3) cell confluency reached 70% within the range of 4–7 days.[2] The last criterion allowed assays to be terminated while cells were in the growth phase. Once optimal conditions were established, each PDCL was reverse transfected in a 384-well plate format with a custom siGENOME siRNA library (Dharmacon, Lafayette, CO) designed to target 714 kinase-coding genes, 256 protein phosphatase-coding genes, 722 genes implicated in energy metabolism, 73 tumor suppressor genes, and 166 genes involved in the repair of DNA damage (see Supplementary Table 19 for a list of genes covered in the siRNA library). Each well in the 384-well plate arrayed library contained a SMARTpool of 4 distinct siRNA species targeting different sequences of the target transcript. Each plate was supplemented with non-targeting siCONTROL and siPLK1 siRNAs (Dharmacon). Cell viability was estimated 5 days after transfection by using a luminescent assay detecting cellular ATP levels (CellTitre-Glo, Promega). Luminescence values were processed by using the cellHTS2 R package.[3] To evaluate the effect of each siRNA pool on cell viability, we log2 transformed the luminescence measurements and then centered these to the median value for each plate. The plate-centered data were scaled to the median absolute deviation of the library as a whole to produce robust Z scores. All screenings were performed in triplicate. Screenings judged to have poor dynamic range (Z' factor < 0)[4] or poorly correlated replicates ($r < 0.7$) were excluded during an evaluation of screening quality. Z scores were adjusted using a quantile normalization.[5]

Small Interfering RNA Screening Analysis

siRNA hits were identified by calculating the median absolute deviation of normalized Z scores for a given siRNA across all samples and identifying sample Z scores greater than or equal to 2 $\times$ the median absolute deviation. This analysis generated a seed matrix (n siRNA hits $\times$ m

samples), which was used as the starting input for the random walk with restart algorithm as implemented by the R package dnet.[6] This algorithm was used to identify functionally important subnetworks associated with cell viability from a curated protein-protein interaction network, STRING, version 10.[7] Considering the complex nature of topologic features of human interactome data, we introduce a randomization-based test to evaluate the candidate interactors using 1000 topologically matched random networks. Candidate interactors that remain significant (ie, $P_{edge} < .05$) were identified, and a consensus subnetwork was constructed by collapsing all sample-specific results. The resulting network was visualized by using RedeR.[8]

RNA-Sequencing Analysis

RNAseq read mapping was performed by using the bcbio-nextgen project RNAseq pipeline (https://bcbio-nextgen.readthedocs.org/en/latest/). Briefly, after quality control and adaptor trimming, reads were aligned to the GRCh37 genome build using STAR[9] counts for known genes were generated by using the function featureCounts in the R/Bioconductor package Rsubread.[10] The R/Bioconductor package DESeq2 was used to normalize count data between samples and to identify differentially expressed genes.[11] Expression data were normalized using the rlog transform in the DESeq2 package, and these values were used for all downstream analyses.

Weighted Gene Coexpression Network Analysis. WGCNA was used to generate a transcriptional network from rlog-normalized RNAseq data.[1] Briefly, WGCNA clusters genes into network modules using a TOM. The TOM is a highly robust measure of network interconnectedness and essentially provides a measure of the connection strength between 2 adjacent genes and all other genes in a network. Genes are clustered by using 1 – TOM as the distance measure and gene modules are defined as branches of the resulting cluster tree using a dynamic branch-cutting algorithm.

Identification of Significant Subtype-Specific Changes in Pathways and/or Processes

The R package clipper[12] was used to identify pathways and/or processes showing significant change between PDCL subtypes. clipper implements a 2-step empirical approach, using a statistical analysis of means and concentration matrices of graphs derived from pathway topologies, to identify signal paths having the greatest association with a specific phenotype.

Pathway Analysis

Ontology and pathway enrichment analysis was performed by using the R package dnet and/or the ClueGO/CluePedia Cytoscape[13,14] plugins as indicated. Visualization and/or generation of network diagrams was performed with either Cytoscape[15] or the R package *RedeR*.[8]

Replication Stress Signature Generation

To define subtype-specific signatures that can inform therapeutic development, differentially expressed genes were compared to genes associated with GO terms by using the R package dnet. Significantly expressed GO terms involved in DDR and cell cycle control were selected. Differential expression of each selected GO term was applied to each individual PDCL that underwent RNAseq. This, in turn, was used to generate a composite score by totaling the score for each selected GO term. The *sig.score* function from the R package genefu[16] was used to calculate a specific signature score in a given sample by using the signatures generated for each pathway and/or process. This was termed the replication stress signature. Generation of signature score for bulk tumor samples followed the same methodology.

Bulk Expression Sets and Immune Signature Scores

Bulk RNAseq expression data, subtype assignments, and immune signature scores were obtained from Bailey et al.[17]

Gene Set Enrichment of Pancreatic Ductal Adenocarcinoma Subtypes

Gene set enrichment was performed by using the R package GSVA.[18] Gene sets representing PDAC subtypes were generated as previously described.[17]

Clustering and Subtype Assignment

The package ConsensusClusterPlus[9] was used to classify PDCLs according to the expression signatures defined in Moffitt et al[20] and Bailey et al.[7] Gene sets representing PDAC subtypes were generated as previously described.

Statistical Analysis

A Kruskal-Wallis test was applied to the indicated stratified scores to determine whether distributions were significantly different. Fisher exact tests were used to evaluate the association between dichotomous variables.

Plot Generation

Heatmaps and oncoplots were generated using the R package ComplexHeatmap.[21] Dot charts, density plots, and boxplots were generated using the R package ggpubr. Violin plots were generated with the Python package *Seaborn*. Biplot was generated by using the R package ggfortify.[22] All other plots were generated using the R package ggplot2.[23]

Patient-Derived Xenograft Therapeutic Testing

PDX of PDAC were generated and comprehensively characterized as part of the ICGC project.[24–26] BALB/c nude mice were anesthetized, and a single PDX fragment was inserted subcutaneously into the right flank according to standard operating procedure. PDX models were grown to 150 mm^3 (volume = [length^2 × width]/2); at this point, each PDX was randomized to a different treatment regime. Responsive PDXs were treated once tumor size returned to 150 mm^3, up to a maximum of 3 rounds. Resistant models were treated after a treatment break of 2 weeks in accordance with current clinical treatment regimes, up to a

maximum of 2 rounds. Each experiment was terminated once tumor volume reached the end point (750 mm^3), in accordance with home office animal welfare regulations.

Upon tumor threshold, mice were treated with either cisplatin, gemcitabine, olaparib, saline (control), or combinations of these (Supplementary Tables 3–4). As PDXs were reaching the threshold, treatment allocation was done on a random basis, with a random number generator. Each PDX was treated with the subsequent treatment regimen upon reaching the threshold depending on the random order generated for that round. This ensured no bias in selecting PDXs to treatments. Phosphate-buffered saline (control) was allocated during every second round of treatments.

Treatment cycles were completed after 4 weeks. If tumor response was observed, then further cycles were given if only tumor growth returned to the threshold (150 mm^3). In cases in which no significant response was seen, a 2-week treatment break was given to all animals, and then a second cycle was restarted. The maximum number of cycles that each animal was exposed to was 3 cycles.

Supplementary References

1. Langfelder P, Horvath S. WGCNA: an R package for weighted correlation network analysis. BMC Bioinformatics 2008;9:559.
2. Campbell J, Ryan CJ, Brough R, et al. Large-scale profiling of kinase dependencies in cancer cell lines. Cell Rep 2016;14:2490–2501.
3. Boutros M, Bras LP, Huber W. Analysis of cell-based RNAi screens. Genome Biol 2006;7(7):R66.
4. Zhang JH, Chung TD, Oldenburg KR. A simple statistical parameter for use in evaluation and validation of high throughput screening assays. J Biomol Screen 1999;4:67–73.
5. Parrish RS, Spencer HJ 3rd. Effect of normalization on significance testing for oligonucleotide microarrays. J Biopharm Stat 2004;14:575–589.
6. Fang H, Gough J. The 'dnet' approach promotes emerging research on cancer patient survival. Genome Med 2014;6(8):64.
7. Szklarczyk D, Franceschini A, Wyder S, et al. STRING v10: protein-protein interaction networks, integrated over the tree of life. Nucleic Acids Res 2015;43(D1):D447–D452.
8. Castro MA, Wang X, Fletcher MN, et al. RedeR: R/Bioconductor package for representing modular structures, nested networks and multiple levels of hierarchical associations. Genome Biol 2012;13(4):R29.
9. Dobin A, Davis CA, Schlesinger F, et al. STAR: ultrafast universal RNA-seq aligner. Bioinformatics 2013;29:15–21.
10. Liao Y, Smyth GK, Shi W. featureCounts: an efficient general purpose program for assigning sequence reads to genomic features. Bioinformatics 2014;30:923–930.
11. Love MI, Huber W, Anders S. Moderated estimation of fold change and dispersion for RNA-seq data with DESeq2. Genome Biol 2014;15(12):550.
12. Martini P, Sales G, Massa MS, et al. Along signal paths: an empirical gene set approach exploiting pathway topology. Nucleic Acids Res 2013;41(1):e19.
13. Bindea G, Galon J, Mlecnik B. CluePedia Cytoscape plugin: pathway insights using integrated experimental and in silico data. Bioinformatics 2013;29:661–663.
14. Bindea G, Mlecnik B, Hackl H, et al. ClueGO: a Cytoscape plug-in to decipher functionally grouped gene ontology and pathway annotation networks. Bioinformatics 2009;25:1091–1093.
15. Shannon P, Markiel A, Ozier O, et al. Cytoscape: a software environment for integrated models of biomolecular interaction networks. Genome Res 2003;13:2498–2504.
16. Haibe-Kains B, Desmedt C, Loi S, et al. A three-gene model to robustly identify breast cancer molecular subtypes. J Natl Cancer Inst 2012;104:311–325.
17. Bailey P, Chang DK, Nones K, et al. Genomic analyses identify molecular subtypes of pancreatic cancer. Nature 2016;531(7592):47–52.
18. Hanzelmann S, Castelo R, Guinney J. GSVA: gene set variation analysis for microarray and RNA-seq data. BMC Bioinformatics 2013;14:7.
19. Wilkerson MD, Hayes DN. ConsensusClusterPlus: a class discovery tool with confidence assessments and item tracking. Bioinformatics 2010;26:1572–1573.
20. Moffitt RA, Marayati R, Flate EL, et al. Virtual microdissection identifies distinct tumor- and stroma-specific subtypes of pancreatic ductal adenocarcinoma. Nat Genet 2015;47:1168–1178.
21. Gu Z, Eils R, Schlesner M. Complex heatmaps reveal patterns and correlations in multidimensional genomic data. Bioinformatics 2016;32:2847–2849.
22. Tang Y, Horikoshi M, Li W. ggfortify: unified interface to visualize statistical result of popular R packages. R J 2016;8:478–489.
23. Wickham H. ggplot2: elegant graphics for data analysis. New York: Springer-Verlag, 2009.
24. Biankin AV, Waddell N, Kassahn KS, et al. Pancreatic cancer genomes reveal aberrations in axon guidance pathway genes. Nature 2012;491(7424):399–405.
25. Waddell N, Pajic M, Patch AM, et al. Whole genomes redefine the mutational landscape of pancreatic cancer. Nature 2015;518(7540):495–501.
26. Bailey P, Chang DK, Nones K, et al. Genomic analyses identify molecular subtypes of pancreatic cancer. Nature 2016;531(7592):47–52.

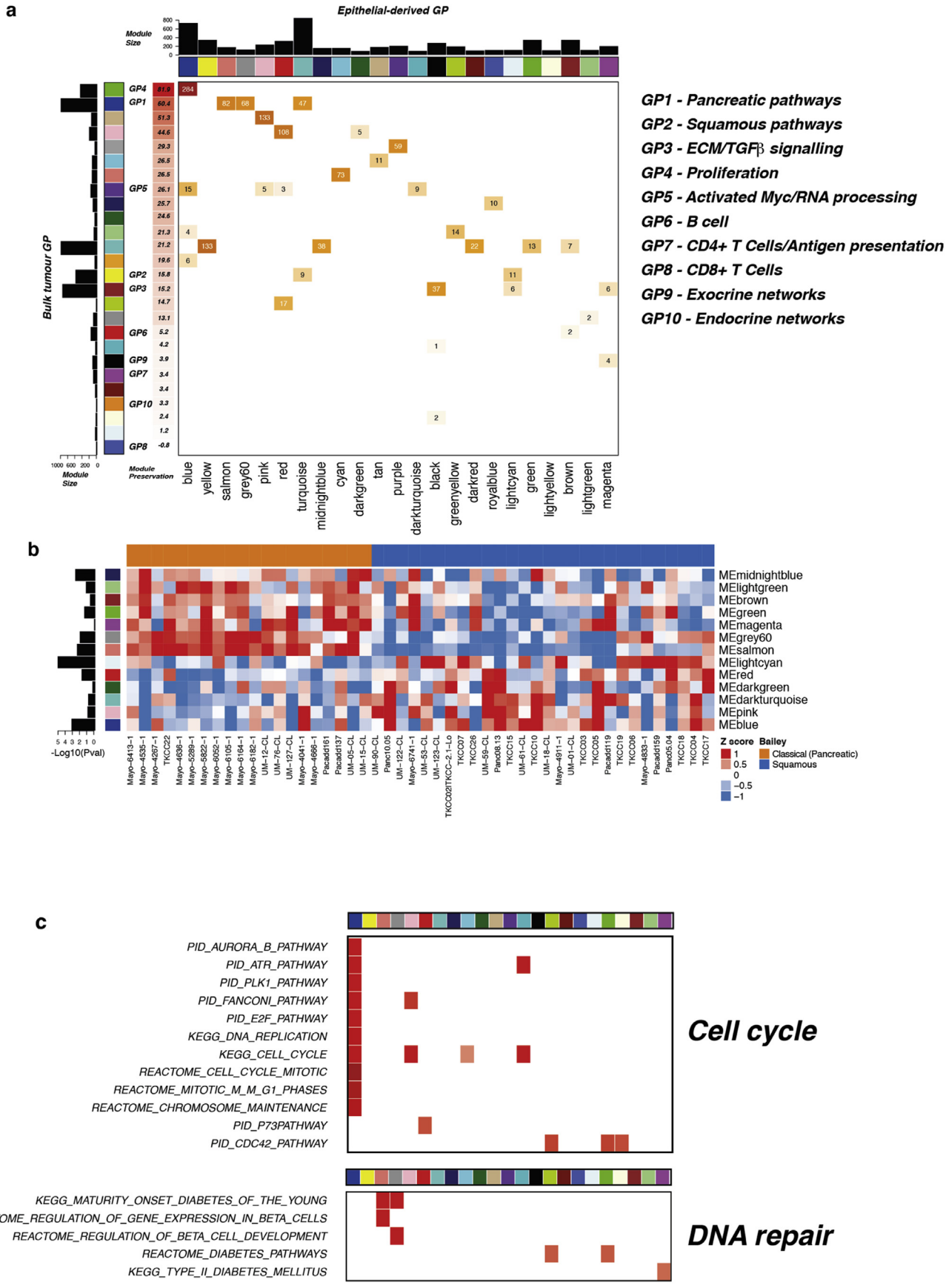
a
Epithelial-derived GP
Module Size
Bulk tumour GP
GP4
GP1
GP5
GP2
GP3
GP6
GP9
GP7
GP10
GP8
Module Preservation
blue
yellow
salmon
grey60
pink
red
turquoise
midnightblue
cyan
darkgreen
tan
purple
darkturquoise
black
greenyellow
darkred
royalblue
lightcyan
green
lightyellow
brown
lightgreen
magenta
GP1 - Pancreatic pathways
GP2 - Squamous pathways
GP3 - ECM/TGFβ signalling
GP4 - Proliferation
GP5 - Activated Myc/RNA processing
GP6 - B cell
GP7 - CD4+ T Cells/Antigen presentation
GP8 - CD8+ T Cells
GP9 - Exocrine networks
GP10 - Endocrine networks
b
-Log10(Pval)
MEmidnightblue
MElightgreen
MEbrown
MEgreen
MEmagenta
MEgrey60
MEsalmon
MElightcyan
MEred
MEdarkgreen
MEdarkturquoise
MEpink
MEblue
Z score
Bailey
Classical (Pancreatic)
Squamous
c
PID_AURORA_B_PATHWAY
PID_ATR_PATHWAY
PID_PLK1_PATHWAY
PID_FANCONI_PATHWAY
PID_E2F_PATHWAY
KEGG_DNA_REPLICATION
KEGG_CELL_CYCLE
REACTOME_CELL_CYCLE_MITOTIC
REACTOME_MITOTIC_M_M_G1_PHASES
REACTOME_CHROMOSOME_MAINTENANCE
PID_P73PATHWAY
PID_CDC42_PATHWAY
Cell cycle
KEGG_MATURITY_ONSET_DIABETES_OF_THE_YOUNG
REACTOME_REGULATION_OF_GENE_EXPRESSION_IN_BETA_CELLS
REACTOME_REGULATION_OF_BETA_CELL_DEVELOPMENT
REACTOME_DIABETES_PATHWAYS
KEGG_TYPE_II_DIABETES_MELLITUS
DNA repair

Supplementary Figure 1. Gene program dysregulation in PC PDCLs. (*A*) Comparison of gene programs (GP) of bulk tumor previously described[28] and GPs identified in PDCLs by WGCNA; ranked by GP module preservation on the *x*-axis. (*B*) Heatmap of PDCLs classified into squamous (*blue*) and classical pancreatic (*orange*) subtypes showing GP module eigengene (ME) values. (*C*) The expression of components of publicly curated molecular pathways and mechanisms in PDCLs related to replication and DNA damage repair. GPs are grouped into key molecular processes that are important in carcinogenesis. ECM, extracellular matrix; TGF, transforming growth factor.

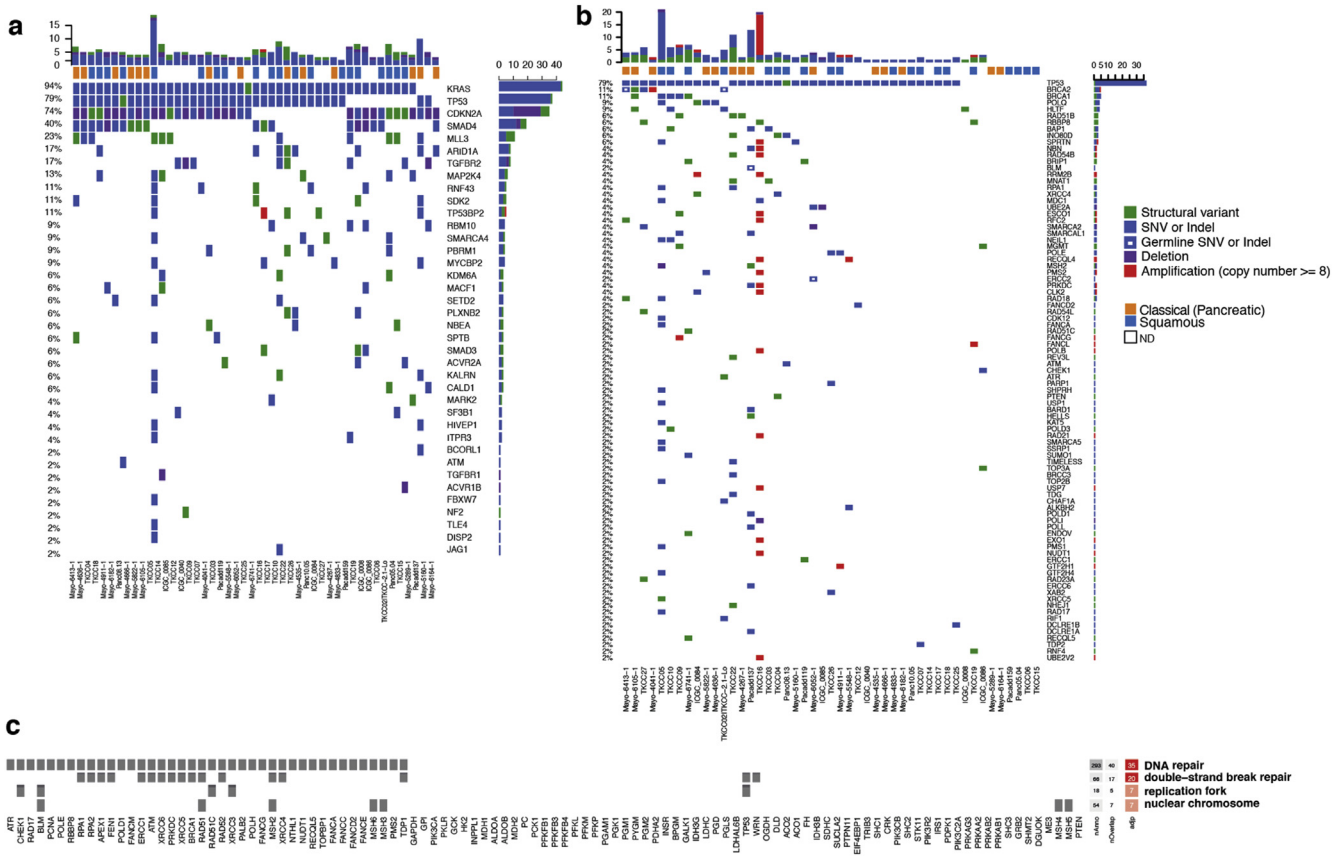

Supplementary Figure 2. Mutational landscape and subtype-specific siRNA screening dependencies of PC PDCLs. (*A*) Oncoplot of somatic mutations of significantly mutated genes in PDCLs. Structural variations (*green*), nonsilent mutations (*blue*), deletion (*purple*), and amplification of $\geq$8 copies (*red*). (*B*) Oncoplot of somatic and germline mutations in key genes known to contribute to DDR and its mutation rate. (*C*) siRNA hits across all PDCLs grouped into molecular processes of DDR.

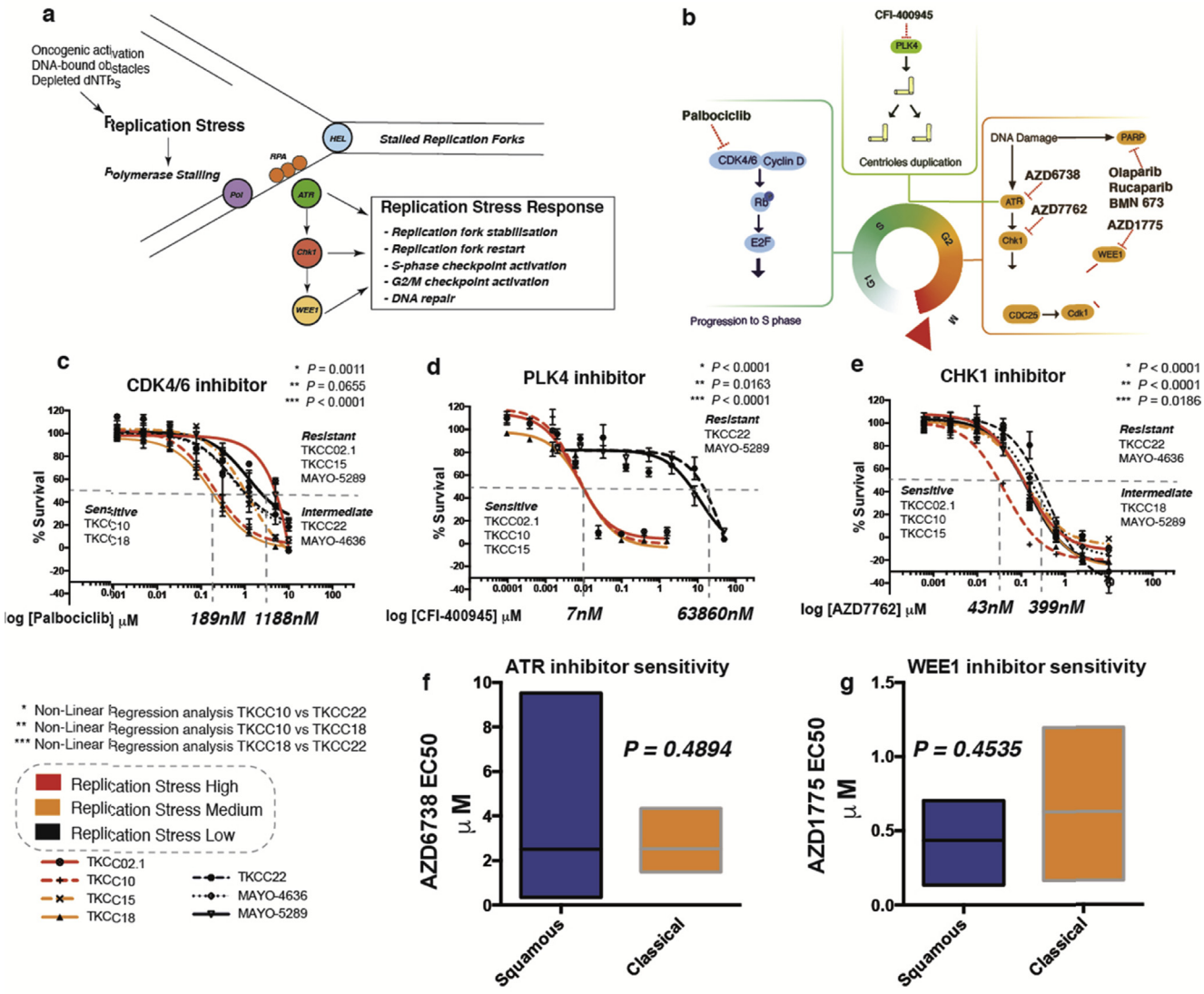

h

PDCL DDR / Replication Status

- High Replication Stress / DDR Deficient
- High Replication Stress / DDR Proficient
- Low Replication Stress / DDR Deficient
- Low Replication Stress / DDR Proficient

Drug Response

- Sensitive
- Resistant

Signature Score

- High
- Low

	Cell line	Replication Stress Score	Replication Stress Rank	Molecular subtype	SV subtype	GPOL HRD Test Positive	BRCA signature rank	DDR Mutations	HRDetect score	*TP53* status	*ATR Inhibitor* AZD6738 EC50 μM	*WEE1 Inhibitor* AZD1775 EC50 μM	*Platinum* Cisplatin EC50 μM
RS High DDR def	TKCC10	9.00	2	Squamous	unstable	1	7	*BRCA1, ARID1A*	0.9957	Mutant	0.345	0.134	3.249
	TKCC02.1	6.26	11	Squamous	unstable	1	1	*BRCA2*	0.9387		0.693	0.605	2.019
	TKCC05	8.09	6	Squamous	scattered	0	6	*BRCA1, RPA1, RAD54L2, FANCA, CK12*	0.1332	Mutant	0.410	0.145	6.231
	Pacadd137	2.57	19	Classical	stable	0	44	*PPPr2R2B, PPPR2R2D, ARID1A*	0.0012	Mutant	1.635	0.164	3.234
	Panc08.13	10.21	1	Squamous	scattered	0	43	*ATM*	0.2545		2.606	0.449	3.140
RS High DDR prof	TKCC15	5.08	13	Squamous	scattered	0	34		0.0126		0.832	0.501	18.72
	TKCC18	4.46	17	Squamous	stable	0	37	*ARID1a*	0.0000	Mutant	1.12	0.364	10.09
	TKCC17	5.07	14	Squamous	scattered	0	20		0.0941	Mutant	2.617	0.272	-
	TKCC07	5.74	12	Squamous	focal	0	13		0.0007	Mutant	2.47	0.605	36.17
RS Lo DDR def	TKCC22	-8.35	41	Classical	unstable	1	5	*RPA1*	0.9989	Mutant	4.332	0.77	6.659
	TKCC26	-6.50	37	Squamous	focal (>200SVs)	0	21	*ARID1A*	0.3327	Mutant	1.757	0.575	5.183
	Mayo-4636	-1.95	29	Classical	scattered	0	10		0.0034	Mutant	2.644	1.195	9.964
RS Lo DDR Prof	Mayo-5289	-3.09	31	Classical	scattered	0	46		0.0182		1.491	0.380	-
	Mayo-4911	2.05	22	Squamous	focal	0	28		0.1382	Mutant	9.52	0.703	9.353
	TKCC06	-0.05	25	Squamous	stable	0	32		0.0002		5.154	-	22.72

Supplementary Figure 3. Targeting replication stress in PC PDCLs. (*A*) Replication stress can be induced by multiple factors, including oncogenic activation (KRAS, MYC) and chemotherapeutics (eg, platinum). This results in stalled replication forks when DNA polymerases (Pol) are separated from DNA helicase (HEL). This results in the coating of single-strand DNA by replication protein A (RPA), which results in ATR activation. This, in turn, generates the replication stress response via CHK1 and WEE1, resulting in checkpoint activation and DNA repair. This safeguards the integrity of the genome by preventing entry into mitosis with incompletely replicated genomes. (*B*) Agents currently in clinical trials or approved for use in other cancer types that target cell cycle checkpoints. Cell viability curves for agents inhibiting (*C*) CDK4/6 (palbociclib), (*D*) PLK4 (CDI-400945), and (*E*) CHK1 (AZD7762). PDCLs were classified by replication stress signature score as high (*red*), medium (*orange*), and low (*black*). (*F*) Differences in sensitivity to ATR inhibitor (AZD6738) in squamous and classical cell lines. (*G*) Differences in sensitivity to WEE1 inhibitor (AZD1775) in squamous and classical cell lines. (*H*) Response to DNA damaging agents and agents targeting cell cycle checkpoint. Colored heatmap reflects replication stress signature score and relative HRDetect score (*red* indicates high; *blue* indicates low) and drug sensitivity (*green* indicates most sensitive; *red* indicates resistant). In general, PDCLs with high replication stress are more sensitive to ATR and WEE1 inhibition, irrespective of DDR status. In general, platinum sensitivity is dependent on DDR status, irrespective of replication stress signature score. dNTP, deoxynucleotide triphosphate.

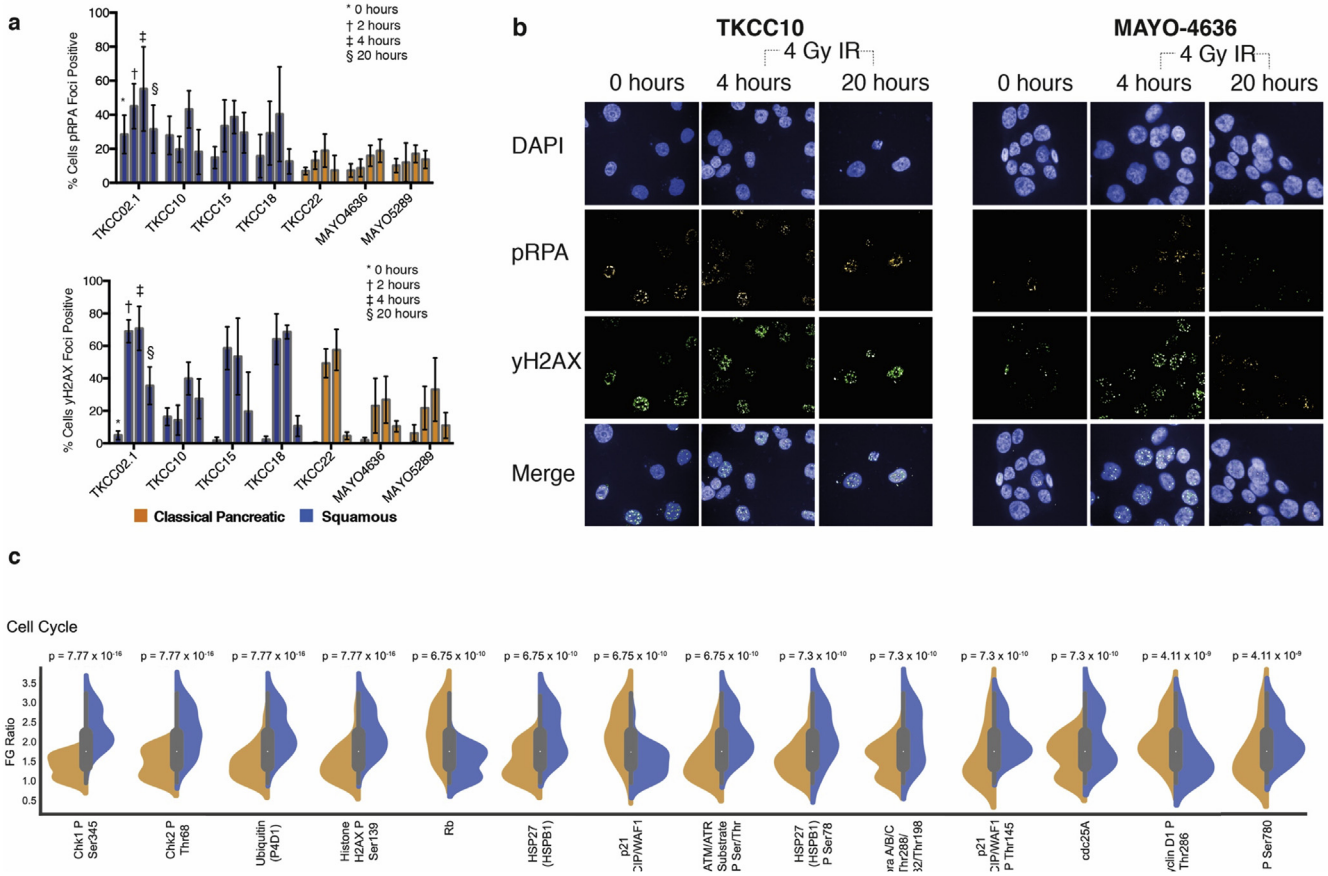

Supplementary Figure 4. Replication stress in PC PDCLs. (*A*) Immunofluorescent quantification of pRPA and yH2AX after 4 Gy of ionizing radiation (IR) in classical pancreatic (*orange*) and squamous (*blue*) PDCLs. pRPA- and γH2AX-positive cells are defined as cells with >10 foci of pRPA and γH2AX per cell. (*B*) Immunofluorescent images of TKCC10 (squamous) and Mayo-4636 (classical pancreatic) PDCLs at normal and at 4 and 20 hours after 4 Gy IR. (*C*) Violin plots of RPPA analysis showing differential expression of (phospho-)proteins in, cell cycle, and DNA damage pathways between subtypes. Kruskal-Wallis test was used for violin plot *P* values. FG, femtogram.

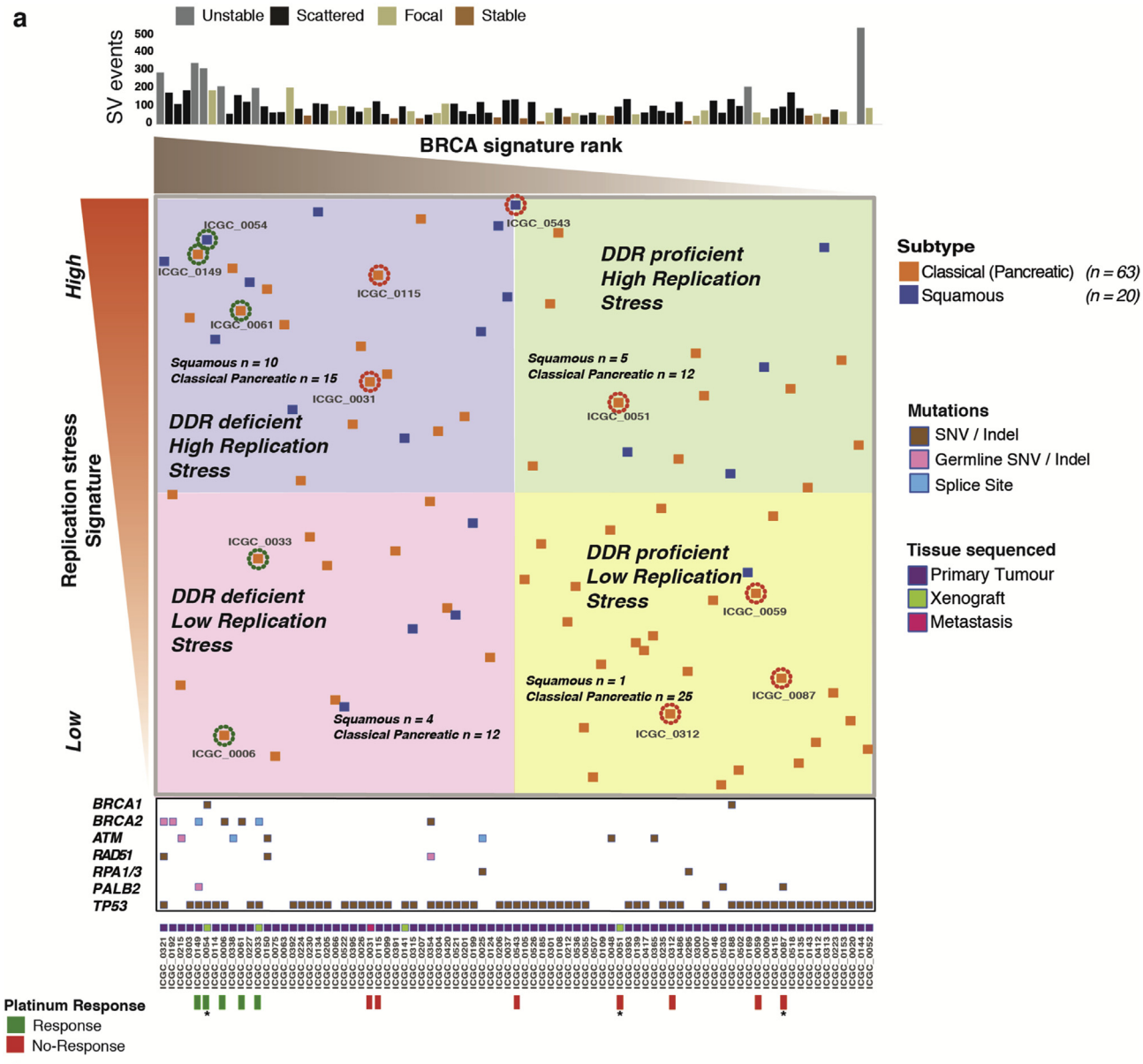
a
Unstable
Scattered
Focal
Stable
SV events
500
400
300
200
100
0
BRCA signature rank
High
Replication stress Signature
Low
DDR proficient High Replication Stress
DDR deficient High Replication Stress
DDR deficient Low Replication Stress
DDR proficient Low Replication Stress
Squamous n = 10
Classical Pancreatic n = 15
Squamous n = 5
Classical Pancreatic n = 12
Squamous n = 4
Classical Pancreatic n = 12
Squamous n = 1
Classical Pancreatic n = 25
ICGC_0054
ICGC_0149
ICGC_0115
ICGC_0061
ICGC_0031
ICGC_0543
ICGC_0051
ICGC_0033
ICGC_0006
ICGC_0059
ICGC_0087
ICGC_0312
BRCA1
BRCA2
ATM
RAD51
RPA1/3
PALB2
TP53
Platinum Response
Response
No-Response
Subtype
Classical (Pancreatic) (n = 63)
Squamous (n = 20)
Mutations
SNV / Indel
Germline SNV / Indel
Splice Site
Tissue sequenced
Primary Tumour
Xenograft
Metastasis
b
PRECISION-Panc EUS Training cohort
Homologous DNA Pairing/Strand Exchange
M/G1 Transition
G2/M DNA damage checkpoint
DNA Damage Recognition in GG NER
Senescence Associated Heterochromatin Foci
Formation of TC NER Pre Incision Complex
G1/S DNA Damage Checkpoints
HDR through Single Strand Annealing SSA
MMR
Recognition of DNA damage: PCNA complex
E2F inhibition of pre replication complex
DNA Replication pre initiation
APC Cdc20 to APC Cdh1 conversion: late anaphase
Chk1 Chk2 inactivation of Cyclin B/Cdk1 complex
Cyclin A/B1 associated events during G2/M transition
Activation of ATR in response to replication stress
Fanconi Anemia Pathway
Mitotic Spindle Checkpoint
Pyrimidine metabolism
Cell cycle
Homologous recombination
Zscore
1
0.5
0
−0.5
−1

Supplementary Figure 5. Targeting replication stress and DDR deficiency in clinical cohorts of PC. (*A*) Bulk tumor samples from the ICGC PC cohort that have undergone both whole-genome sequencing and RNAseq are ranked from left to right based on the COSMIC BRCA mutational signature as a scale of DDR deficiency (*x*-axis) and top to bottom by the novel transcriptomic signature of replication stress (*y*-axis). HR pathway gene mutations and source of tissue sequenced are marked along the *x*-axis. Platinum response is marked along *x*-axis, and the related patient is encircled at individual points, where green represents response, and red indicates resistance. An asterisk indicates PDX response data. Relevant molecular subtype frequency (squamous vs classical pancreatic) is indicated for each quadrant, showing that squamous PC was associated with high-ranking replication stress score (15 out of 41 vs 5 out of 42) ($P = .009$, chi-square test). (*B*) The replication stress signature in the Precision-Panc endoscopic ultrasonography fine-needle biopsy training cohort, showing its clinical utility in the advanced disease setting (34% of cohort was locally advanced, and 37% was metastatic). The top-ranking quartile of replication stress signature scored as high showed that 50% of squamous tumors were within this group, compared to only 21% of the classical pancreatic tumors ($P = .027$, chi-square test). EUS, endoscopic ultrasonography; SNV, single-nucleotide variant.

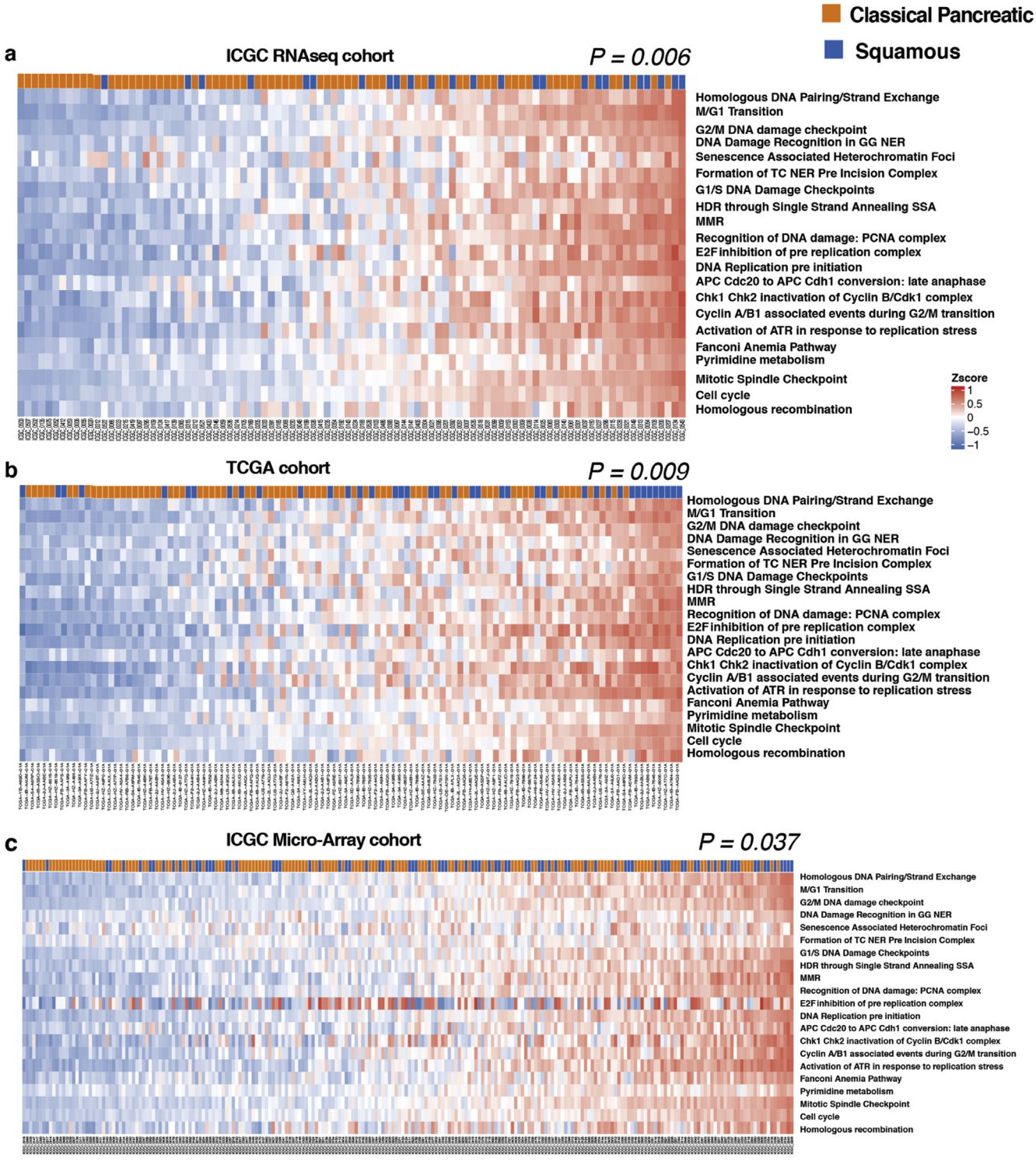

Supplementary Figure 6. Replication stress signature in published bulk tumor cohorts of PC. The association between molecular subtype and replication stress in the (*A*) ICGC RNAseq (n = 94), (*B*) TCGA (n = 112), and (*C*) ICGC microarray (n = 232) cohorts. In the ICGC ($P = .006$), TCGA ($P = .009$), and ICGC microarray cohorts ($P = .037$), high replication stress was significantly enriched for the squamous subtype. High replication stress was defined as the top-ranking quartile in this cohort; *P* was calculated using the chi-square test.